

# Transport Studies on CVD-Grown Graphene

by

Miriam Hanna Huntley

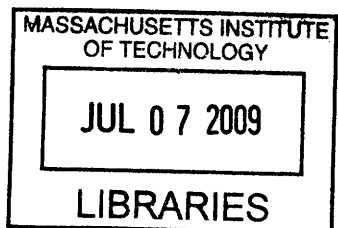
Submitted to the Department of Physics  
in partial fulfillment of the requirements for the degree of  
Bachelor of Science in Physics

# MASSACHUSETTS INSTITUTE OF TECHNOLOGY

June 2009

© Miriam Hanna Huntley, MMIX. All rights reserved.

The author hereby grants to MIT permission to reproduce and distribute publicly paper and electronic copies of this thesis document in whole or in part.



Author ... ..... Department of Physics  
May 21, 2009

Certified by . . . , .....  
Raymond C. Ashoori  
Professor of Physics  
Thesis Supervisor

Accepted by ..... David E. Pritchard  
Cecil and Ida Green Professor of Physics, Department Senior Thesis  
Coordinator



# **Transport Studies on CVD-Grown Graphene**

by

Miriam Hanna Huntley

Submitted to the Department of Physics  
on May 21, 2009, in partial fulfillment of the  
requirements for the degree of  
Bachelor of Science in Physics

## **Abstract**

In this thesis, we report transport studies performed on CVD-grown graphene. We perform resistivity and hall measurements on a large-area sample at 4° K. We measure the carrier mobility of the sample and find it to be on the order of  $1000 \text{ cm}^2/\text{Vs}$ , whereas monolayer graphene regularly exhibits much higher mobilities. We also examine what we find to be weak signatures of Shubnikov-de Haas oscillations in magnetic field sweeps. Finally, we study magneto-resistance effects at low fields, and find that the sample exhibits weak-localization effects.

Thesis Supervisor: Raymond C. Ashoori  
Title: Professor of Physics



## Acknowledgments

I owe many thanks to many people for the work that was carried out here. First and foremost, I am supremely grateful to my advisor, Prof. Ray Ashoori, for allowing me to take on this project and work through it my own way, even if that way was not always the best. His guidance and enthusiasm, combined with his deep intuition for thinking about many of the issues that came up, were invaluable. This project would never have been successful without the continual help of both Dr. Lu Li and Dr. Oliver Dial, the two postdoctorate fellows working in the group. I would like to thank them both for their willingness to help me run the experiment (especially at ungodly hours of the night) and for generously giving of their time in order sit down and talk with me about the results. I also owe thanks to Anjan Soumyanarayanan and Eric Lin for advice on some of the glitches that came up, as well as to Dr. Michele Zaffalon for discussions about weak localization. Thanks is also due to Prof. Robert Jaffe for discussions about notation choice in the tight-binding model of graphene.



# Contents

|          |   |           |
|----------|---|-----------|
| <b>1</b> | <b>Introduction</b>                                 | <b>13</b> |
| 1.1      | A Brief History of Graphene . . . . .               | 14        |
| 1.2      | Dispersion Relation . . . . .                       | 16        |
| 1.2.1    | Derivation . . . . .                                | 16        |
| 1.2.2    | Interpreting the Energy Spectrum . . . . .          | 21        |
| 1.3      | Quantum Hall Effect in Graphene . . . . .           | 22        |
| 1.3.1    | Review of Integer Quantum Hall Effect . . . . .     | 22        |
| 1.3.2    | Anomalous Quantum Hall Effect in Graphene . . . . . | 25        |
| 1.4      | Localization Effects in Graphene . . . . .          | 26        |
| 1.5      | Other Recent Discoveries . . . . .                  | 28        |
| 1.5.1    | Potential Uses for Graphene . . . . .               | 29        |
| 1.6      | CVD-grown Graphene . . . . .                        | 31        |
| <b>2</b> | <b>Experimental Methods</b>                         | <b>35</b> |
| 2.1      | Goals . . . . .                                     | 35        |
| 2.2      | Van Der Pauw Technique . . . . .                    | 35        |
| 2.3      | Hall Measurement . . . . .                          | 37        |
| 2.4      | Sample Preparation . . . . .                        | 37        |
| 2.5      | Experimental Setup . . . . .                        | 39        |
| 2.6      | Controlling the Experiment . . . . .                | 40        |
| 2.7      | Experimental Parameters . . . . .                   | 41        |

|   |           |
|---|-----------|
| <b>3 Results</b>  | <b>45</b> |
| 3.1 Raw Data . . . . .  | 45        |
| 3.1.1 Voltage Sweeps . . . . .                                | 45        |
| 3.1.2 Magnetic Field Sweeps . . . . .                         | 51        |
| 3.2 Symmetrization and Antisymmetrization Averaging . . . . . | 51        |
| 3.3 Annealing Effects . . . . .                               | 55        |
| 3.4 Mobility Measurements . . . . .                           | 55        |
| 3.5 Shubnikov-de Haas Oscillations . . . . .                  | 61        |
| <b>4 Conclusion</b>   | <b>65</b> |
| 4.1 Future Studies . . . . .                                  | 65        |
| 4.2 Summary . . . . .   | 65        |

# List of Figures

|   |    |
|---|----|
| 1-1 A pictorial representation of graphene. The two dimensional substance is made up of carbon atoms arranged on a hexagonal lattice. Graphene is also the building block of carbon materials in other dimensions: 0D buckeyballs, 1D nanotubes, and 3D graphite. From [7]. . . . .   | 14 |
| 1-2 Electrons on white (A) sites can only hop to black (B) sites, and vice versa. Any linear combination of $\vec{a}_1$ and $\vec{a}_2$ will connect any two arbitrary A sites, while there is a B site located $\vec{\delta}$ above every A site. Some of the position states are labelled (the label appears in all cases above the site it describes). . . . . | 17 |
| 1-3 Energy dispersion relation of Equation (1.18) on the left, with a close-up on the right of one of the Dirac points about which there is a linear spectrum. From [15]. . . . .   | 20 |

|  |    |
|--|----|
| 1-4 Landau level energies plotted along D(E), the density of states. On the left, the Landau levels for electrons in a material obeying a parabolic energy spectrum are shown. The levels are equally spaced and occur at integer filling factors, and we can write the energy of a level in terms of the filling factor $\nu$ : $E_\nu = \hbar\omega_c(\nu + 1/2)$ (where $\omega_c$ is the cyclotron frequency). On the right, the Landau levels for graphene are shown. The lowest Landau level is equally filled by holes (blue) and electrons (red) and lies at E=0. In graphene, the Landau levels are not equally spaced because the energy spectrum is no longer proportional to $\nu$ but rather to its square root: $E_\nu = \sqrt{2 e B\hbar v_F^2(\nu + 1/2 \pm 1/2)}$ (where the final $\pm 1/2$ depends on whether the level is in the upper or lower band, and $B$ is the magnetic field). From [10]. . . . . | 26 |
| 1-5 The quantum Hall effect of graphene. $n$ is the 2D number density and is positive for electrons and negative for holes. Note that at certain values of $n$ there are zeros in the longitudinal resistivity, corresponding with plateaus in the Hall conductivity at half-integers of $4e^2/h$ . From [7] . . . . .   | 27 |
| 1-6 Tunneling as a particle approaches a barrier is shown for graphene (top) and for conventional semiconductors (bottom). The size of the sphere is meant to indicate the amplitude of the wave function. As can be seen, in graphene the transmission probability is close to one. From [10]. . . . .  | 31 |
| 1-7 Optical image of the CVD-grown graphene samples used for this study. Regions of the light-pink (i.e. the ‘background’ color) have 1-2 layer thickness, while other regions have more layers. Scale is in microns. . . . .  | 34 |
| 2-1 Using the van der Pauw technique, one makes two sets of measurements to determine $R_A$ and $R_B$ , from which one can then find the sheet resistance of the material. Image from [13]. . . . .  | 36 |

|      |   |    |
|------|---|----|
| 2-2  | Optical image of a piece of graphene scraped to suit our measurement needs. . . . .   | 42 |
| 2-3  | Here we show a representation of our experimental setup. The lock-in signal output was sent to one of the graphene contacts, with another contact grounded. The remaining two contacts provided our voltage signal, measured by the lock-in. The backgate was biased to change the makeup of the charge carriers. . . . . | 43 |
| 2-4  | The graphene sample used for these studies, with the four silver-epoxy contacts labeled. Scale is in microns. . . . .   | 44 |
| 2-5  | Two measurement configurations shown for a VDP measurement $V_{14,23}$ on the left and a cross measurement $V_{13,42}$ on the right. The other two, not shown, were the second VDP configuration ( $V_{12,43}$ ) and the second crossed configuration ( $V_{24,31}$ ). . . . .  | 44 |
| 3-1  | Raw data for the first VDP configuration, $V_{14,23}$ . . . . .   | 46 |
| 3-2  | Raw data for the second VDP configuration, $V_{14,23}$ . . . . .  | 47 |
| 3-3  | Raw data for the first crossed configuration, $V_{13,42}$ . . . . .   | 49 |
| 3-4  | Raw data for the second crossed configuration, $V_{24,31}$ . . . . .  | 50 |
| 3-5  | Raw data for magnetic sweep at two backgate voltages, $V_{bg}=55.6$ V and $V_{bg}=25$ V, both measuring $V_{24,31}$ . . . . .   | 52 |
| 3-6  | Weak localization effect seen at zero backgate voltage at 100 mK. . . .   | 53 |
| 3-7  | Weak localization effect seen at $V_{bg}=25$ V at 4 K. . . . .  | 54 |
| 3-8  | $V_{24,31}$ data for +10 T, -10 T, and the antisymmetric average of the two. .  | 56 |
| 3-9  | Sheet resistance $R_S$ evaluated with the symmetrized VDP averages. .   | 57 |
| 3-10 | Mobility calculated via the VDP traces as a function of the density. While mobility really only carries meaning at zero field, we here also show the mobility derived at 10 and 4 T to show the large density behavior. . . . .   | 58 |
| 3-11 | Mobility calculated via the VDP traces on the electron side. . . . .  | 59 |

|   |    |
|---|----|
| 3-12 The difference between subsequent data points in $R_{xy}$ (for $V_{bg} = 50$ V) plotted as a function of the inverse magnetic field. The green is interpolated data, needed in order to have evenly spaced data in inverse magnetic field for the fourier transform. . . . . | 62 |
| 3-13 Fourier transform of the data shown in Figure 3-12 . . . . .   | 63 |

# Chapter 1

## Introduction

Graphene, a one-atom-thick layer of carbon atoms arranged on a hexagonal lattice, has emerged within the past five years as an increasingly important topic in the scientific world. To put this trend in context, consider the following: before the year 2004, the number of papers published in Physical Review Letters with the word "graphene" either in their title or abstract numbered less than fifty. The number of papers published since then has reached over one thousand, and shows no sign of abating. The reason for the enormous amount of interest that graphene has generated lies in its unique properties and tantalizing possibilities. There is still much to be done in terms of fully characterizing and understanding this remarkable substance.

In this thesis, we review our results from transport measurements performed on a graphene sample that was grown by a particular method called chemical vapor deposition (CVD). The motivation for this work stemmed partially from the fact that very few measurements of the type performed here have been carried out on CVD-grown graphene until now, and transport studies are an important way of characterizing the material that can yield valuable information.

This thesis is organized as follows: In the rest of this chapter, we provide background on graphene, from both theory and experimental viewpoints. We briefly review its history, and then derive and discuss some of its unique properties, including its linear dispersion relation and its display of the so-called ‘anomalous’ quantum Hall effect. In Chapter 2, we review the experimental methods that were used in

this study, providing details on the sample preparation, the four-probe measurement technique, and the experimental setup. In Chapter 3 we will present the results of our study and discuss their implications. Finally, we will conclude with thoughts on future paths of research for CVD-grown graphene.

## 1.1 A Brief History of Graphene

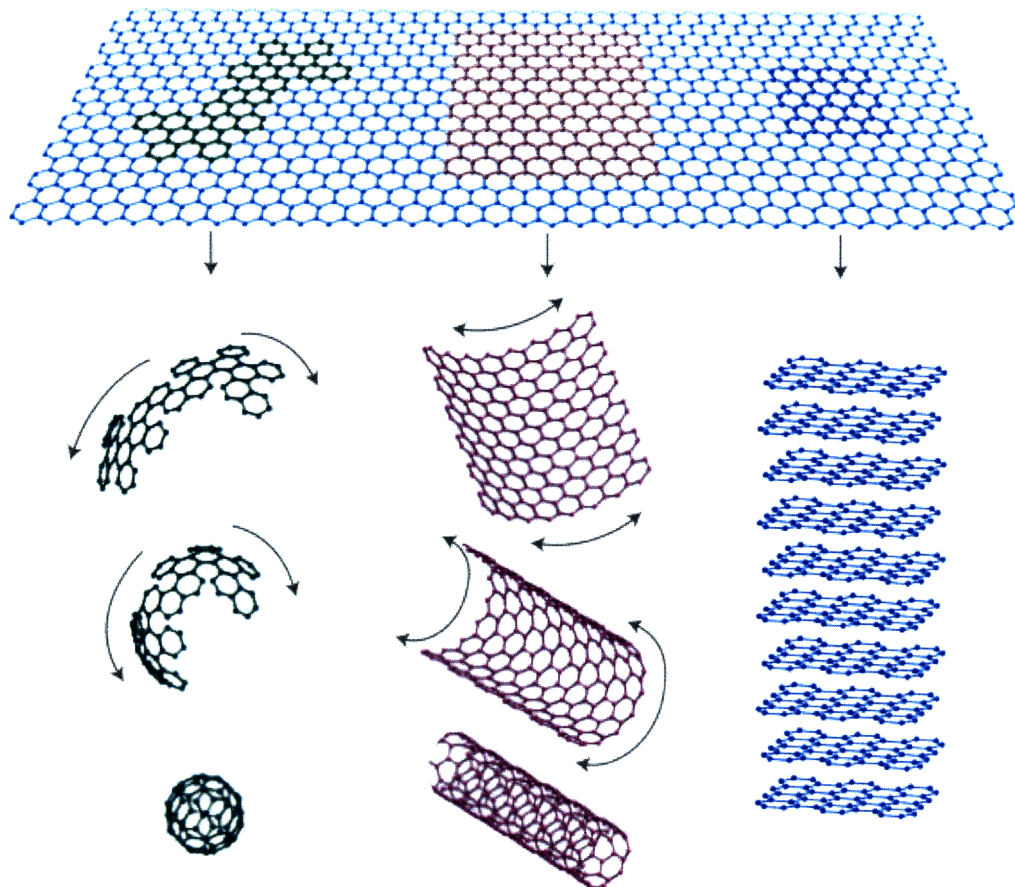


Figure 1-1: A pictorial representation of graphene. The two dimensional substance is made up of carbon atoms arranged on a hexagonal lattice. Graphene is also the building block of carbon materials in other dimensions: 0D buckeyballs, 1D nanotubes, and 3D graphite. From [7].

Graphene is a one-atom-thick substance, made up of carbon atoms arranged on a honeycomb lattice (see Figure 1-1). The carbon atoms, which have four valence

electrons, bond together with three symmetric  $sp^3$ -orbitals, leaving one electron free on every atom in a  $p$ -orbital perpendicular to the plane. Much of the discussion surrounding graphene involves studying how these electrons in the  $p$ -orbitals conduct: how does the periodic array of carbon atoms affect them? How do they react when an electric field is applied? When a magnetic field is applied? And so forth.

Graphene, for many years, was thought impossible to create. Graphite is a common substance in nature, and consists of many layers of graphene stacked upon one another. However, many convincing arguments have been made, most notably by Lev Landau [12], that show that a two-dimensional structure cannot be thermally stable and therefore cannot exist. Nevertheless, though graphene was not studied experimentally for a long time, many of its unique properties have been well known for decades, though only relevant to theorists. In 1947, Phillip R. Wallace published a paper discussing graphene's energy dispersion relation (that is to say, the relation between the energy of eigenstates of the Hamiltonian,  $E$ , and the wave vector  $\vec{k}$ ) [27]. Using the tight-binding model, Wallace showed that at certain  $\vec{k}$  points, the energy goes linearly with changes in  $\vec{k}$ . This linear dispersion relation, also known as a Dirac dispersion relation, differs substantially from the usual  $E(\vec{k}) \sim |\vec{k}|^2$ . This unique spectrum was thought to be an interesting oddity, though of course impossible to probe experimentally.

It came as a rather shocking surprise, then, when a group at Manchester University, led by Andre Geim and Kostya Novoselov, succeeded in 2004 in creating graphene [16, 17, 6], the first two-dimensional crystal ever produced. Taking a rather simple approach of just using some scotch tape to separate the layers of graphite over and over again, the Oxford group was able to isolate a single layer of graphene. Their subsequent measurements on the substance not only confirmed Wallace's prediction of a linear dispersion relation but also uncovered interesting physics that is still being probed today. With many rich features, along with certain properties that make it promising for development in the electronics industry, it took very little time after its debut into the world of experimental physics for graphene to become the darling of experimental and theoretical physicists alike.

We will now address some of graphene's unique properties, starting with its linear dispersion relation, in more detail.

## 1.2 Dispersion Relation

### 1.2.1 Derivation

To derive the linear dispersion relation for graphene, we will employ the tight-binding method in order to reproduce the results found by Wallace over sixty years ago. In the tight-binding model, one assumes that the localized wave functions of electrons on an isolated atom are known. Then, when multiple atoms are brought together to form a lattice, we assume that the interaction between atoms is small such that the wave functions stay more or less the same; the electrons are still forced to live in these localized wave functions, or position states, located at the lattice points. However, the effect of bringing the atoms together gives electrons a small but non-zero probability of tunneling from one position state to the next, and it is this tunneling that allows the electrons to conduct.

For this derivation, we will create localized states in which electrons can reside, each atom having one state. We will assume that electrons can only tunnel to nearest-neighbor position states. The distance between any two adjacent sites on the lattice is denoted as  $a$ , and the tunneling matrix element which allows for hopping between nearest neighbor sites in the Hamiltonian is  $-\Delta$ .

To move forward with this method, one must come up with a method of labeling the localized wave functions. To start, we examine a pictorial representation of the sites (Figure 1-2), where we have colored sites either black or white. We see that if an electron is on a black site (a 'B' site), all of its nearest neighbors are white, so it can only hop to white sites (or 'A' sites). Similarly, an electron on a white site can only tunnel to a black site. This motivates us to distinguish between the black and white sites in our labeling.

If we look only at the white sites, we see that they form a trigonal sub-lattice. We

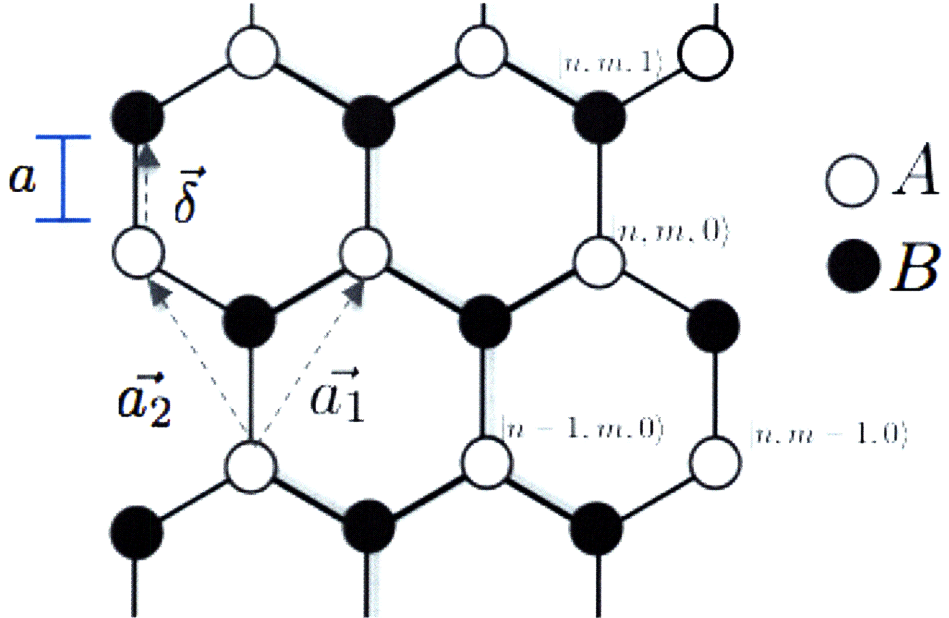


Figure 1-2: Electrons on white (A) sites can only hop to black (B) sites, and vice versa. Any linear combination of  $\vec{a}_1$  and  $\vec{a}_2$  will connect any two arbitrary A sites, while there is a B site located  $\vec{\delta}$  above every A site. Some of the position states are labelled (the label appears in all cases above the site it describes).

can describe the location of every site as a linear combination of two vectors,  $\vec{a}_1$  and  $\vec{a}_2$ , where  $\vec{a}_1 = a(\frac{\sqrt{3}}{2}, \frac{3}{2})$  and  $\vec{a}_2 = a(-\frac{\sqrt{3}}{2}, \frac{3}{2})$ . If we define our origin to be at some arbitrary white site, the position vector of every other white site can be written as  $\vec{r} = n\vec{a}_1 + m\vec{a}_2$ , where  $n$  and  $m$  are integers. The black sites form a trigonal sub-lattice as well, but one that is vertically shifted upwards from the white sub-lattice. For instance, if there is a white site at  $\vec{r} = n\vec{a}_1 + m\vec{a}_2$ , then there is a black site above it at  $\vec{r} = n\vec{a}_1 + m\vec{a}_2 + \vec{\delta}$ , where  $\vec{\delta} = a(0, 1)$ .

Using these vector definitions, we will choose to label our states as  $|n, m, l\rangle$ , which will represent a site that is displaced from the origin by  $\vec{r} = n\vec{a}_1 + m\vec{a}_2 + l\vec{\delta}$ , where  $n$  and  $m$  can take on any integer value, and  $l$  can be either 0 or 1. Note that if  $l = 0$ , the site in question is a white site (an 'A' site), while if  $l = 1$  it must be a black site (a 'B' site). We can formalize this notation by showing how certain operators act on the position states (we will not need these operators for the rest of the paper, but

they are provided here for clarification purposes):

$$\hat{r} |n, m, l\rangle = (n\vec{a}_1 + m\vec{a}_2 + l\vec{\delta}) |n, m, l\rangle \quad (1.1)$$

$$\hat{A} |n, m, 0\rangle = |n, m, 0\rangle \quad (1.2)$$

$$\hat{A} |n, m, 1\rangle = 0 \quad (1.3)$$

$$\hat{B} |n, m, 0\rangle = 0 \quad (1.4)$$

$$\hat{B} |n, m, 1\rangle = |n, m, 1\rangle \quad (1.5)$$

where the  $\hat{A}$  and  $\hat{B}$  operators tell us if we are on an A or B site, respectively.<sup>1</sup>

With this formality set up, we can now define a translation operator. Looking at the graph, we see that if an electron is sitting on the white site  $|n, m, 0\rangle$ , it can only go to  $|n, m, 1\rangle$ ,  $|n - 1, m, 1\rangle$ , and  $|n, m - 1, 1\rangle$  (which are the B sites that are respectively above, below to the left, and below to the right of the original A site).

Thus we can write, summing over all possible white sites an electron can start out in,

$$\hat{T} = \sum_{n,m} (|n, m, 1\rangle + |n - 1, m, 1\rangle + |n, m - 1, 1\rangle) \langle n, m, 0|. \quad (1.6)$$

We analogously can create the translation operator for electrons that start on black sites and hop to white sites:

$$\hat{T}^\dagger = \sum_{n,m} (|n, m, 0\rangle + |n + 1, m, 0\rangle + |n, m + 1, 0\rangle) \langle n, m, 1|. \quad (1.7)$$

We then write our Hamiltonian as

$$\hat{H} = -\Delta(\hat{T} + \hat{T}^*) \quad (1.8)$$

where  $\Delta$  moderates the strength of the hopping and we have set to zero the energy

---

<sup>1</sup>It should be noted that there are a few different ways one can go about deriving the dispersion relation for graphene, which all of course give the same results in the end. My choice of notation here differs substantially from Wallace's original paper, and in fact does not follow any one author specifically but rather emerged largely from a discussion I had with Professor Robert Jaffe. For a derivation which follows from a more standard, solid-state physics perspective, see [26]. For a more general discussion of two different (yet equivalent) choices of translation vectors, see [1].

common to all localized states.

To find the eigenvalues of this Hamiltonian, we will first need to find the eigenstates. Bloch's theorem in two dimensions tells us that if there is a periodic potential on the lattice such that  $V(\vec{r}) = V(\vec{r} + \vec{G})$  (i.e. if you are at position  $\vec{r}$  then the potential looks exactly that same if you translate away by the vector  $\vec{G}$ ), then any wave function which satisfies the following equation will be eigenstate of the Hamiltonian:

$$\psi_{\vec{k}}(\vec{r} + \vec{G}) = e^{i\vec{k}\cdot\vec{G}}\psi_{\vec{k}}(\vec{r}) \quad (1.9)$$

(where  $\vec{k}$  is the two-dimensional wave vector). As we did in the 1D case, we will create a superposition of position states. We first define:

$$|\psi_{\vec{k}}^A\rangle = \sum_{n,m} e^{i\vec{k}\cdot(n\vec{a}_1 + m\vec{a}_2)} |n, m, 0\rangle \quad (1.10)$$

$$|\psi_{\vec{k}}^B\rangle = \sum_{n,m} e^{i\vec{k}\cdot(n\vec{a}_1 + m\vec{a}_2 + \vec{\delta})} |n, m, 1\rangle \quad (1.11)$$

If we then write

$$|\psi_{\vec{k}}\rangle = c_A |\psi_{\vec{k}}^A\rangle + c_B |\psi_{\vec{k}}^B\rangle, \quad (1.12)$$

where  $c_A$  and  $c_B$  are some constants yet to be chosen,  $|\psi_{\vec{k}}\rangle$  will satisfy Bloch's equation and therefore be an eigenstate of the system. This gives us:

$$\hat{H} |\psi_{\vec{k}}\rangle = E(\vec{k}) |\psi_{\vec{k}}\rangle. \quad (1.13)$$

From this point, standard way to derive  $E(\vec{k})$  is to take the inner product of Equation (1.13) above and two single electron states,  $\langle i, j, 0 |$  and  $\langle i, j, 1 |$ . This gives us, after canceling common exponential factors, the following two equations:

$$-\Delta e^{-i\vec{k}\cdot\vec{\delta}}(1 + e^{-i\vec{k}\cdot\vec{a}_1} + e^{-i\vec{k}\cdot\vec{a}_2})c_B = E(\vec{k})c_A \quad (1.14)$$

$$-\Delta e^{i\vec{k}\cdot\vec{\delta}}(1 + e^{i\vec{k}\cdot\vec{a}_1} + e^{i\vec{k}\cdot\vec{a}_2})c_A = E(\vec{k})c_B \quad (1.15)$$

We can now write the effective Hamiltonian in the A, B basis as:

$$\hat{H} = - \begin{pmatrix} 0 & \Delta e^{-i\vec{k}\cdot\vec{\delta}}(1 + e^{-i\vec{k}\cdot\vec{a}_1} + e^{-i\vec{k}\cdot\vec{a}_2}) \\ \Delta e^{i\vec{k}\cdot\vec{\delta}}(1 + e^{i\vec{k}\cdot\vec{a}_1} + e^{i\vec{k}\cdot\vec{a}_2}) & 0 \end{pmatrix} \quad (1.16)$$

which gives us

$$E(\vec{k}) = \pm \Delta |1 + e^{i\vec{k}\cdot\vec{a}_1} + e^{i\vec{k}\cdot\vec{a}_2}| \quad (1.17)$$

or, after plugging in the appropriate vectors and a little trigonometric manipulation,

$$E(\vec{k}) = \pm \Delta \sqrt{3 + 2 \cos(\sqrt{3}ak_x) + 4 \cos\left(\frac{\sqrt{3}}{2}ak_x\right) \cos\left(\frac{3}{2}ak_y\right)} \quad (1.18)$$

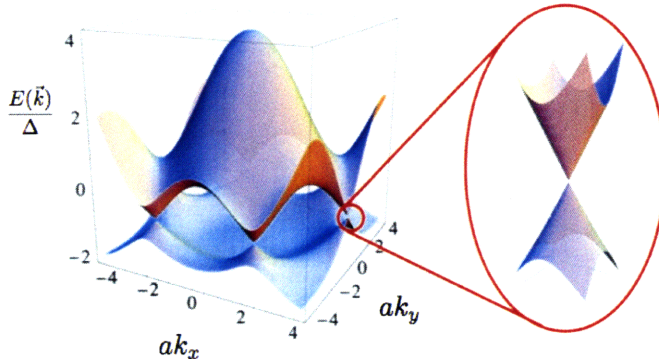


Figure 1-3: Energy dispersion relation of Equation (1.18) on the left, with a close-up on the right of one of the Dirac points about which there is a linear spectrum. From [15].

Figure 1-3 is a plot of Equation (1.18), with the energy as a function of  $k_x$  and  $k_y$ . We see that the two bands (i.e. the '+' and '-' branches of the solution) touch at 6 distinct points in k-space, which are called Dirac points. Where the two bands touch,  $E(\vec{k}) = 0$  of course, and, as it turns out, around these 6 points the energy goes linearly with perturbations in  $\vec{k}$ . This is the origin of the linear dispersion relation.

We can prove more quantitatively that the energy does indeed go linearly with disturbances in  $\vec{k}$ . Let's look at one of the Dirac points where the two bands meet,  $\vec{k}_0 = \frac{1}{a}(\frac{4}{3\sqrt{3}}\pi, 0)$ . We will look at the space near  $\vec{k}_0$  such that  $\vec{k} = \vec{k}_0 + \delta\vec{k}$  for small

$\delta\vec{k}$ . We could expand the energy relation in Equation (1.18) to obtain the desired linear relation, but it will be instructive to expand the Hamiltonian itself of Equation (1.16). This then gives us to first order in  $\delta\vec{k}$ :

$$\hat{H} = -\frac{3}{2a}\Delta \begin{pmatrix} 0 & \delta k_x - i\delta k_y \\ \delta k_x + i\delta k_y & 0 \end{pmatrix} \quad (1.19)$$

However, the above equation is usually written out in the following manner (exchanging the constant  $\Delta$  for more preferable constants):

$$\hat{H} = \hbar v_F \sigma \cdot \vec{k} = \hbar v_F \begin{pmatrix} 0 & \delta k_x - i\delta k_y \\ \delta k_x + i\delta k_y & 0 \end{pmatrix} \quad (1.20)$$

where  $\sigma$  is the 2D Pauli matrix and  $v_F$  is the fermi velocity of the electrons. In this form the Hamiltonian is exactly analogous to the Dirac Hamiltonian for massless relativistic particles, with just an interchange of  $v_F$ , the Fermi velocity, with  $c$ , the speed of light. The well-known linear dispersion relation results from solving for the eigenvalues:

$$E(\delta\vec{k}) = \pm \hbar v_F \sqrt{\delta k_x^2 + \delta k_y^2} = \pm \hbar v_F |\delta\vec{k}| \quad (1.21)$$

as drawn on the right hand side of Figure 1-3.

It is hard to overstate the importance of this result. Almost everywhere one looks in condensed matter physics, particles tend to obey dispersion relations that are proportional to  $k^2$ . Though there is nothing relativistic about the motion of electrons in graphene, they obey the same Hamiltonian as do massless relativistic particles. This property of graphene has generated an enormous amount of interest in the substance.

### 1.2.2 Interpreting the Energy Spectrum

One of the important consequences of this unique energy spectrum is the tunability it lends to graphene [7]. The position of the Fermi energy determines the makeup of the carriers. At  $E_F = 0$ , exactly between the two branches, there are no carriers

(no holes and no electrons). However, the Fermi energy can be moved up or down by applying a backgate voltage on the graphene, and thereby inducing a change (over many orders of magnitude) in the number of holes or the number of electrons. This is remarkably simple compared to what is done in semiconductors, where one has to chemically dope the material in order to create a sizeable change in the number or type of carriers.

## 1.3 Quantum Hall Effect in Graphene

### 1.3.1 Review of Integer Quantum Hall Effect

The classical Hall effect, discovered by Edwin Hall in 1879 [8], is a well understood phenomenon of electricity and magnetism and has been used as a standard measurement tool in the electronics industry for decades. The derivation of the Hall effect is as follows: suppose we have a two-dimensional conductor upon which we will be applying electric or magnetic fields, which has either positive or negative charge carriers (holes or electrons). We can define the conductivity  $\sigma$  and resistivity  $\rho$  of the material using the corresponding tensors:

$$\vec{j} = \sigma \vec{E} \quad (1.22)$$

$$\rho = \sigma^{-1} \quad (1.23)$$

where  $\vec{j}$  is the current density and  $\vec{E}$  is the applied electric field, and  $\rho$  is the inverse of the conductivity tensor. In the x-y basis we can write the conductivity tensor as (with no assumptions about sample isotropy)

$$\sigma = \begin{pmatrix} \sigma_{xx} & -\sigma_{xy} \\ \sigma_{xy} & \sigma_{yy} \end{pmatrix} \quad (1.24)$$

Carrying out the matrix inversion, one then has

$$\rho_{xy} = \frac{\sigma_{xx}}{\sigma_{xx}^2 + \sigma_{xy}^2} \quad (1.25)$$

$$\rho_{xx} = \frac{\sigma_{xy}}{\sigma_{xx}^2 + \sigma_{xy}^2} \quad (1.26)$$

Let us consider the case where we have current traveling only in the x-direction of the sample. If a magnetic field  $\mathbf{B} = B\hat{\mathbf{z}}$  is applied perpendicular to the plane the charge carriers will experience a Lorentz force. This Lorentz force will push the carriers in the direction transverse to the current and the magnetic field in the  $+y$ , regardless of the charge of the carriers. Charge will build up on one side of the conductor, causing voltage in the transverse (y) direction. This voltage will eventually balance out the Lorentz force such that the charge carriers can go back to traveling only in the  $\hat{x}$  direction as if the B field was not present.

The voltage across the y-direction is called the Hall voltage  $V_H$  and is a measurable quantity. Since we require the Hall voltage to exactly cancel the magnetic field's effect, one can show that

$$V_H = \frac{IB}{nq} \quad (1.27)$$

where  $n$  and  $q$  are the the 2D number density and charge of the carriers and  $d$  is the thickness of the conductor. The Hall conductivity is defined as

$$\sigma_{xy} = \frac{j_x}{E_y}, \quad (1.28)$$

which one finds is just equal to

$$\sigma_{xy} = \frac{nq}{B}, \quad (1.29)$$

giving the conductivity a linear dependence in  $n/B$ . Similarly one finds for the Hall resistivity

$$\rho_{xy} = \frac{B}{nq}. \quad (1.30)$$

It was discovered by Klaus von Klitzing in 1980 that at low temperatures and high magnetic field strengths, the Hall conductivity becomes quantized. With an

appropriate treatment of the system using quantum mechanics, the quantization of the Hall coefficients can we be well understood. The essential result of this treatment is that the energy states for charge carriers are split into Landau levels (LL), with Landau levels spaced far enough away from each other that they are distinguishable (at low energies). Each LL has some finite width in energy, but we assume that at low energies the width of the LL is small compared to the spacing between neighboring LL's.

Each Landau level can hold  $D$  charge carriers, where  $D = g\Phi/\Phi_0$ . Here  $\Phi$  is the magnetic flux through the sample,  $\Phi_0 = \frac{h}{e}$  is the magnetic flux quantum, and  $g$  is the degeneracy in  $k$  ( $g = 2$  for particles with spin, while  $g = 4$  in graphene since we have two type of particles with two spin states). In the standard integer quantum Hall effect, the LL's are evenly spaced in energy and go linearly with the number density.

To understand the quantization, let us examine what happens when we fill this energy spectrum with electrons. We start out with no electrons, and begin putting them in one by one. At first, electrons will start to fill the first (lowest) landau level. As we continue to put more and more electrons into the system, eventually the lowest landau level will be filled up. This happens when  $N_e/D = 1$ , where  $N_e$  is the number of electrons. The subsequent electrons will be forced to occupy the next landau level, which will have higher energy. Again, when that level is saturated, there will be a jump to the subsequent level.

Clearly, when  $N_e/D = \nu$ , where  $\nu$  is a positive integer, we have  $\nu$  landau levels that are exactly filled. (One also uses the nomenclature that we have filled the  $0^{th}$  LL up to the  $N^{th}$  LL, where  $N = \nu - 1$ .) Additionally, if  $N_e/D = \nu$ , we have (plugging into our classical derivation of the Hall coefficients)

$$\sigma_H = \nu \frac{e^2}{h} \quad (1.31)$$

$$\rho_{xy} = \frac{h}{e^2 \nu}. \quad (1.32)$$

This tells us that at *specific* values of the electron density, one has conductivity and resistivity being equal to an integer multiple of these fundamental constants. Now as

one varies  $N$ , the conductivity and resistivity will not stay at these quantized values but increase or decrease as appropriate by Equations 1.29 and 1.30. However, it turns out that if the sample has some imperfections (as all samples do), then due to the presence of localized states, the value of the conductivity and resistivity do in fact remain quantized. These localized states are states where the electrons are trapped or ‘pinned down’ by the local potential. Electrons in these states cannot move, so do not contribute to the conductivity.

Performing again a mental ‘filling’ of electrons into the system again, we can see that the effect of these localized states is very important. Let us suppose that you have filled  $\nu$  states already with electrons. As you continue to add electrons, these electrons fill localized states that lie between the  $N$  and  $N + 1$  LL’s, and, as mentioned above, electrons in localized states do not contribute to conduction. Thus, the conductivity remains the same even though we are adding electrons. It is only when electrons begin filling the next Landau level that they can conduct, and so the conductivity and resistivity change. After filling up this level, the values of  $\sigma_{xy}$  and  $\rho_{xy}$  will again remain the same even as we increase the number of electrons, until yet another Landau level is reached. One can also show that when  $\sigma_{xy}$  and  $\rho_{xy}$  are at these special quantized values, we have both  $\sigma_{xx=0}$  and  $\rho_{xx} = 0$ .

Thus we see that as a function of the number of electrons, we will see plateaus in both  $\sigma_{xy}$  and  $\rho_{xy}$  corresponding to their quantization at filled Landau levels. The Landau levels are evenly spaced in electron number  $N_e$  (or, equivalently, in electron density  $n$ ).

### 1.3.2 Anomalous Quantum Hall Effect in Graphene

The “Hallmark of massless Dirac fermions” [7] is considered to be its display of the ‘anomalous quantum Hall effect’. In a simple parabolic energy spectrum, the energy of the  $N$ th Landau level can be written as  $E_N \sim N$ . In graphene, on the other hand, one finds that a straightforward result of the linear energy spectrum (see [15]) is that the Landau levels actually have energy  $E_N \sim \sqrt{N}$ . In addition, the Hall conductivity,  $\sigma_{xy}$ , is no longer quantized at integer multiples of  $\frac{e^2}{h}$  but rather at half

integer multiples of  $\frac{4e^2}{h}$ . The Manchester group was the first to report these properties of graphene [18], and it is this effect that is often seen as the most convincing ‘proof’ that the electrons in graphene actually do follow a linear dispersion relation.

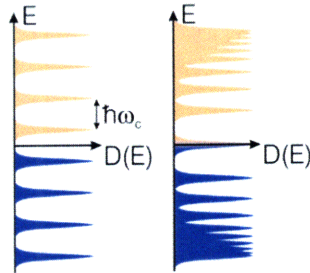


Figure 1-4: Landau level energies plotted along  $D(E)$ , the density of states. On the left, the Landau levels for electrons in a material obeying a parabolic energy spectrum are shown. The levels are equally spaced and occur at integer filling factors, and we can write the energy of a level in terms of the filling factor  $\nu$ :  $E_\nu = \hbar\omega_c(\nu + 1/2)$  (where  $\omega_c$  is the cyclotron frequency). On the right, the Landau levels for graphene are shown. The lowest Landau level is equally filled by holes (blue) and electrons (red) and lies at  $E=0$ . In graphene, the Landau levels are not equally spaced because the energy spectrum is no longer proportional to  $\nu$  but rather to its square root:  $E_\nu = \sqrt{2|e|B\hbar v_F^2}(\nu + 1/2 \pm 1/2)$  (where the final  $\pm 1/2$  depends on whether the level is in the upper or lower band, and  $B$  is the magnetic field). From [10].

The Manchester group also found that graphene, unlike any other substance that had hitherto been seen, exhibits the quantum Hall effect at room temperature [18]. This was an astounding case of a very quantum mechanical trait appearing at ‘classical’ temperatures, and is understood to come from graphene’s high electronic quality.

## 1.4 Localization Effects in Graphene

At high enough temperatures, one can describe electrical conduction in terms of classical descriptions. However, once temperatures are sufficiently low, one must begin to take into account quantum effects. One such quantum effect is called weak localization, a phenomenon that causes extra backscattering during conductance and therefore increases the resistance. The source of this enhanced scattering in the backwards direction is as follows: two charge carriers which travel around a closed loop

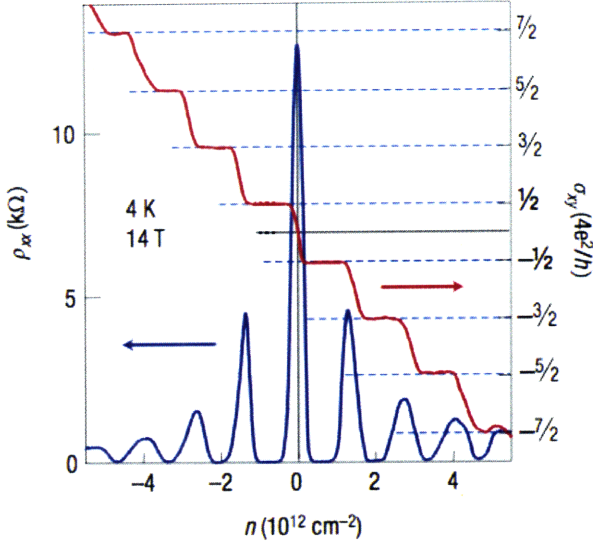


Figure 1-5: The quantum Hall effect of graphene.  $n$  is the 2D number density and is positive for electrons and negative for holes. Note that at certain values of  $n$  there are zeros in the longitudinal resistivity, corresponding with plateaus in the Hall conductivity at half-integers of  $4e^2/h$ . From [7]

in opposite directions will acquire the same phase, and therefore can, once they have returned to their point of origin, constructively interfere in the backwards direction. This effect is suppressed in the presence of a magnetic field because the time-reversal symmetry is broken. Thus in most metals one finds an increase in the magnetoresistance at zero magnetic field which weakens as the field strength is increased.

The case with graphene is somewhat different. Because of the chiral nature of the carriers (which comes from the two interlocked sub-lattices A and B of graphene), theory predicts that if electrons travel in opposite directions around a closed path without being scattered from one valley in  $k$ -space to another valley, the two paths end up destructively, and not constructively, interfering with each other, thereby reducing backscattering. This suppression of backscattering is called weak antilocalization. The condition for weak antilocalization is  $\tau_{intra} \ll \tau_{inter}$ , where  $\tau_{intra}$  is the intravalley elastic scattering time and  $\tau_{inter}$  is the intervalley scattering time. Conversely, if  $\tau_{inter} \ll \tau_{intra}$ , ordinary weak antilocalization will occur.

Experimentally, it has been found that in monolayer graphene, all localization

effects are strongly suppressed, though at high carrier concentrations one sees signatures of weak localization. The reason for this is still under debate and not well understood theoretically. [15]

## 1.5 Other Recent Discoveries

Many groups have confirmed that the charge carriers in graphene have very high mobilities. Electron (or hole) mobility is conventionally seen as a measure of the scattering in the substance: the better the mobility, the smaller the resistivity, and therefore the less loss of energy due to heating during conduction. With mobilities up to  $20,000 \text{ cm}^2/\text{V s}$  [10], graphene beats modern silicon transistors by at least an order of magnitude. Moreover, suspended graphene (as opposed to graphene lying on a silicon-oxide substrate, which is the more common form), has been reported to exhibit even higher mobilities of up to  $200,000 \text{ cm}^2/\text{V s}$  [3] due to a lack of interaction between the electrons and the substrate imperfections and phonons.

As mentioned above, when the Fermi energy is at zero (i.e. when there is no backgate voltage), there are no carriers in the graphene, as we are sitting exactly on a Dirac point. One therefore would expect that the conductivity, which is proportional to the number of carriers, would be zero as well, while the resistivity would diverge. However, it was discovered that the conductivity in graphene never falls below a well-defined minimum. This minimum conductivity, or analogously, maximum resistivity, remains to be thoroughly explained [7]. To complicate matters further, while in theory the number of carriers is supposed to go to zero when the backgate voltage is zero, it turns out that disorder in a graphene sample will shift the Dirac or ‘charge-neutrality’ point [15] such that one must apply a backgate voltage in order to reach the point of minimum conductivity.

Other properties of graphene are still being studied and have yet to be fully understood. The role of disorder in graphene and its ramifications for transport, the effects of phonons on transport, and the mechanism of electron-electron interactions are all examples of topics in graphene research that are still open to debate [15].

There are also many intriguing properties of graphene that in the interest of brevity will not be discussed in this paper. For a very thorough and recent review of the state of graphene theory, see [15]. Graphene is still considered a substance with many rich and interesting physics yet to be discovered, and the quest for understanding its properties has earned it a wide and intense following within the scientific community.

### 1.5.1 Potential Uses for Graphene

The recent excitement over graphene comes in large part from its potential applications. Graphene's high mobility at room temperature has made it a possible candidate for silicon's replacement in the electronics industry. Graphene's mobility at room temperature does not depend strongly on the number of carriers or on chemical doping [7], about which the same cannot be said for modern silicon transistors. Graphene's robust and high mobility has piqued the interest of electrical engineers who hope to use graphene to create faster electronic chips. The high electron mobility in graphene implies large mean-free paths even at room temperature, meaning that electrons can travel large length scales before scattering. By making graphene devices on the order of a micron, ballistic transport, or scattering-free conduction, can be achieved. Engineers have not been able to achieve the same with silicon transistors, because of silicon's smaller mean free path and fabrication challenges which present miniaturization limitations (see [23] for example). If ballistic graphene transistors were to be achieved, electrons would conduct much more efficiently because they would not lose as much energy through heating. Moreover, with ballistic transport, electrons move much faster, and so higher switching frequencies, and therefore faster computing speeds, can be realized. Some studies of graphene transistors have already been performed [16] but it still remains to be seen how useful a device they will be.

It should be mentioned that bilayer graphene has also presented itself as a worthy material for investigation in the field of electronics. One can derive via the tight-binding method the energy spectrum of bilayer graphene, and it turns out that the electrons in bilayer graphene behave like ‘massive Dirac fermions’ and have more tunable properties than electrons in single layer graphene [20]. For instance, by

applying an electric field, one can create a gap between the upper and lower branches of the energy spectrum. This enhanced ability to control the spectrum, along with bilayer graphene's high mobilities [14], has made it a candidate for the next building block of transistors as well.

Another use for graphene is derived from its unique energy spectrum. Although there is nothing relativistic about the motion of the electrons in graphene (they are only traveling at 1/300th's of the speed of light [10]), the electrons mimic what are called massless Dirac particles. In quantum mechanics, particles generally obey the Schrodinger equation. However, when relativistic effects become important, one must combine special relativity with quantum mechanics, which yields a new wave equation: the Dirac equation. For a free particle, Dirac's equation reads:

$$(\beta mc^2 + \alpha_1 \hat{p}_1 + \alpha_2 \hat{p}_2 + \alpha_3 \hat{p}_3) \Psi(\vec{r}, t) = i\hbar \frac{\partial \Psi(\vec{r}, t)}{\partial t} \quad (1.33)$$

where the  $\alpha_i$  are four by four matrices. One can see that if the particle has no mass, the energy will scale linearly with the momentum, i.e.  $E \sim \vec{k}$ .

Physcists don't have many opportunities to experimentally probe the physics of the Dirac equation, nor the physics of quantum electrodynamics (QED), also known as the quantum relativistic field theory of electrodynamics. Graphene therefore has become a playground for physicists to study these areas without the usual costs involved in actually accelerating up the particles to relativistic energies (see [7], [10] for a more thorough discussion). For example, with graphene one can study QED in curved space, a realm which has important significance in cosmology. Another avenue of investigation has focused on better understanding scattering properties of relativistic particles. In non-relativistic quantum mechanics, a particle incident on a potential barrier has a decaying probability of tunneling through the barrier, as is well known. In relativistic quantum mechanics, on the other hand, the situation is drastically different. In 1929, it was discovered by physicist Oskar Klein ([11], [9]) that for a relativistic particle approaching a barrier, if the barrier height  $V_0$  exceeds the particle's rest mass energy, the transmission probability only depends weakly on

$V_0$  and in fact tends to one as  $V_0$  becomes large. Dubbed the ‘Klein Paradox’ for its counterintuitive result, this phenomenon may become better understood through studies on graphene, where experiments studying electron scattering are relatively easy to set up.

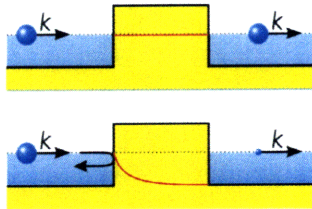


Figure 1-6: Tunneling as a particle approaches a barrier is shown for graphene (top) and for conventional semiconductors (bottom). The size of the sphere is meant to indicate the amplitude of the wave function. As can be seen, in graphene the transmission probability is close to one. From [10].

## 1.6 CVD-grown Graphene

The biggest obstacle facing both the study of graphene and the development of graphene-related devices is one of fabrication. The reason we have not seen the emergence of a ‘Graphene Valley’, so to speak, lies in the fact that no one can make graphene in an inexpensive, scalable, and reproducible manner. There are a few different methods currently being employed by the groups studying graphene, though none yet perfected.

One such method is ‘mechanical exfoliation’, which is the rather generous term given to the scotch-tape method mentioned above (sometimes also referred to as micromechanical cleavage). So simple an undergrad can do it, it is also probably the method of choice for groups wishing to perform physics research on graphene. However, besides for being a tedious process, this technique produces graphene samples of very small areas (on the order of  $100 \mu\text{m}$  wide) in ragged and unpredictable shapes [16], making it unsuitable for applications in industry.

Another approach for creating graphene involves epitaxial growth. The epitaxial

growth method takes a substrate and uses it as a seed crystal for growing the graphene on top of it [2]. This method, however, can yield graphene of non-uniform thickness (i.e. multiple layers) and create unwanted bonding between the bottom graphene layer and the substrate. In addition, epitaxial growth in general requires ultra-high vacuum conditions and is rather expensive.

A third method that has recently emerged is growing the graphene via chemical vapor deposition (CVD). This method is currently being developed by three independent research groups, headed by Jing Kong at MIT, Byung Lee Hong of Sungkyunkwan University, and Yong Chen at Purdue University and shows promise for becoming an effective method of fabrication [19]. The measurements for this study were carried out on samples fabricated by the Kong group, so we here outline the growth process that they employ (see [25] for more details).

A film of polycrystalline nickel is first e-beam evaporated onto  $\text{SiO}_2/\text{Si}$  substrates. The Ni is heated to  $900 - 1000^\circ \text{ C}$ , and then exposed to a highly diluted hydrocarbon flow under ambient pressure. Carbon atoms are thereby generated at the nickel surface, and then diffuse into the metal. The nickel is then cooled down, which causes the carbon atoms to precipitate out to the surface of the nickel and form graphene, in some regions as one layer and in other regions as up to 12 layers.

In order to perform useful measurements on the graphene it is essential to be able to transfer it to other materials. This is accomplished by the Kong group by first applying poly[methyl methacrylate] (PMMA) to the graphene surface, and then treating the film with an aqueous HCl solution which wet etches the underlying Ni film away. This yields a free-standing PMMA/graphene membrane. The membrane is transferred to the substrate of choice and the PMMA is then dissolved off with acetone.

The CVD method is powerful in that it creates very large sheets of graphene (on the order of  $\text{cm}^2$ ), but the graphene is not of uniform thickness. The largest regions of the graphene which consist only of a single layer are only around  $20 \mu\text{m}$  wide. These regions are interrupted by regions with multiple (up to 12) layers of graphene (see Figure 1-7). The morphology of the graphene corresponds with the morphology of

the Ni substrate: the regions of graphene of constant thickness resemble the granular regions of the Ni. It is hoped therefore that by adjusting the morphology of the Ni films, the CVD method will more effectively be able to control the graphene growth such that only mono layer regions are created.

Very little work has been done to date on the large-scale graphene samples. Transport studies of the type performed here have been done for the samples created by the Korea group, but only on monolayer regions within the sample and not on the bulk material itself [5]. Some characterization studies have been carried out by the Kong group [25], but not at the temperatures or magnetic fields explored in this project.

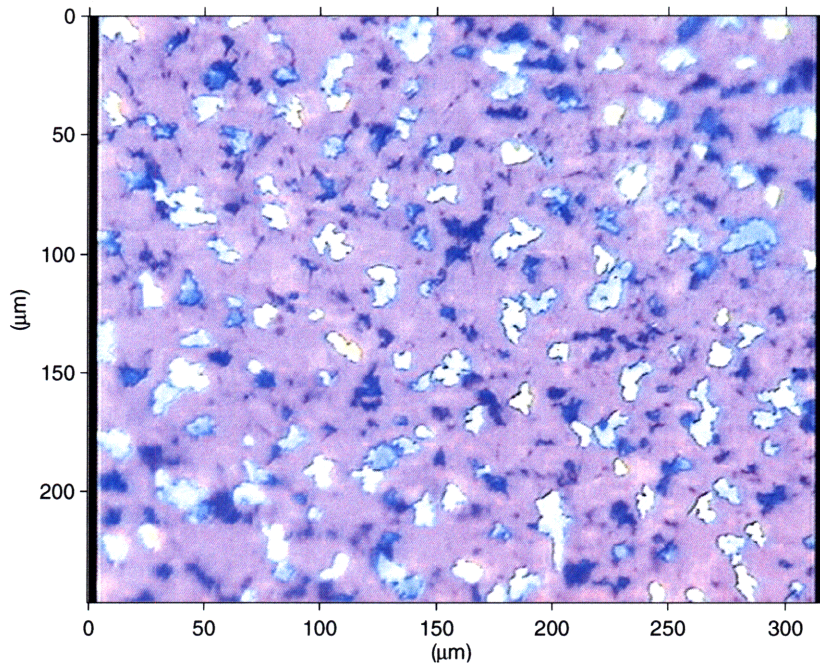


Figure 1-7: Optical image of the CVD-grown graphene samples used for this study. Regions of the light-pink (i.e. the ‘background’ color) have 1-2 layer thickness, while other regions have more layers. Scale is in microns.

# Chapter 2

## Experimental Methods

### 2.1 Goals

The goal of these transport studies was to characterize the CVD-grown graphene. The large-area samples that are created via this method have regions of single-layer graphene as well as regions of multi-layer graphene. How does this mixed composition affect the transport of the substance? There are a number of important quantities one can measure to characterize the material. First, we wished to measure the carrier mobility of the sample: does it have the same high mobility values measured for single layer graphene? Second, we wanted to study the effect of a magnetic field on the sample. Does the material exhibit the anomalous quantum Hall effect? Can Shubnikov-de-Hass oscillations be seen? The third question that we wished to address was that of weak localization: what scattering mechanism dominates in the sample?

We will here discuss the various methods and techniques used to carry out these measurements, as well as explain our experimental setup.

### 2.2 Van Der Pauw Technique

Determining the sheet resistance  $R_S$  of the graphene sample is useful for characterizing the material. Not only does it provide information about the sample's electrical quality, but it can also be used to calculate the mobility  $\mu$  of the material. The method

that we use to measure the sheet resistivity is called the van der Pauw technique, a type of four-probe measurement developed in the fifties [22] and now a standard technique in the semiconductor industry.

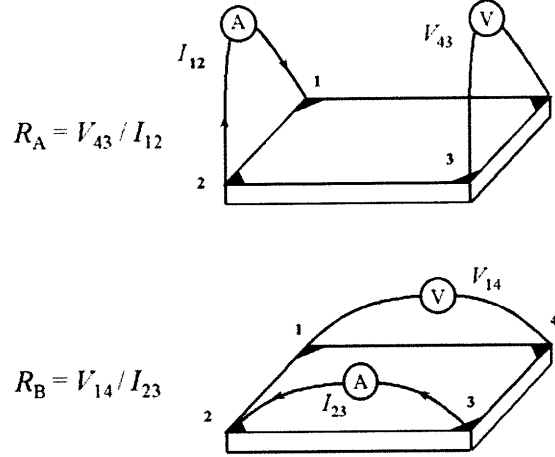


Figure 2-1: Using the van der Pauw technique, one makes two sets of measurements to determine  $R_A$  and  $R_B$ , from which one can then find the sheet resistance of the material. Image from [13].

In this technique, one measures an arbitrarily shaped material by first attaching to it four contacts, preferably on its periphery. If we number our contacts 1-4, the measurement would proceed as follows. We pick two adjacent contacts, say 1 and 2, and pass a small current,  $I_{12}$ , between them. We then measure the voltage between the remaining two contacts,  $V_{43}$ , and define a resistance  $R_A = V_{43}/I_{12}$ . Repeating this measurement with another set of contacts, we similarly measure  $R_B = V_{14}/I_{23}$ . Van der Pauw showed that, regardless of the shape of the material, for a uniform sample with relatively small-sized contacts, one has

$$e^{-\pi R_A/R_S} + e^{-\pi d R_B/R_S} = 1 \quad (2.1)$$

where  $R_S$  is the sheet resistance of the material. Thus by doing two sets of four-probe measurements on our graphene sample, we can determine the sheet resistivity of the graphene. Equation 2.1 does not have an analytical solution and must therefore be

solved numerically.

## 2.3 Hall Measurement

As explained in Chapter 1, the Hall measurement yields the number density  $n$  of the material. Performing this measurement is relatively easy using the same setup as was used for the van der Pauw measurements. In this measurement, after a magnetic field  $B$  is turned on, a current  $I$  is forced between two opposing (i.e. non-adjacent) contacts, and the voltage between the other two opposing contacts,  $V_H$ , is then measured. We can then calculate the number density  $n$  as

$$n = \frac{IB}{qV_H}, \quad (2.2)$$

where the sign of  $V_H$  tells us if the charge carriers are holes or electrons.

Knowing  $n$  from the Hall measurement and  $R_S$  from the VDP method, we can then extract the mobility:

$$\mu = \frac{1}{qnR_S} \quad (2.3)$$

## 2.4 Sample Preparation

The samples we received from the Kong group consisted of the CVD graphene sitting on top of 300 nanometers of SiO<sub>2</sub> and a silicon substrate underneath. The graphene oftentimes ‘spilled’ over the edges of the chip, so in order to electrically isolate a piece of the sample we had to scrape out a piece of the graphene. This was accomplished by using the needles on a probe station to scratch out a smaller square of graphene from the larger piece. This method worked well because the needles on the probe station can be finely controlled and the scratching only lifts off the graphene and does not scratch the oxide below (see Figure 2-2).

After scratching out a square of graphene suitable for measurement, we put contacts onto the four corners of the square. The process of making robust contacts for the sample ended up being somewhat more difficult than we had anticipated. Our

first approach was to use gold wires and to attach them to the corners of the sample using silver paint. It was difficult to put the contacts on by hand (i.e. holding the wire with tweezers and placing carefully on the sample) so we chose to use a more accurate approach which utilized the lab's wire bonder. By putting a drop of the silver paint on the end of the silver wire that was being held by the wire bonder, we then lowered the wire to the desired location and held the wire there until the paint dried. This method was much more reliable in terms of keeping the contacts small and having more precision in placement. We also used the wire bonder to add more paint if any of the contacts seemed mechanically unstable. Again we put a drop of the paint on the end of the wire-bonder wire and used it as a 'brush' to accurately place the extra paint on the desired contact.

Unfortunately, oftentimes these silver paint contacts were not robust. They tended to pop off very easily, especially at lower temperatures. To this effect, we decided to try silver epoxy contacts instead. We could not use the wire bonder to place these contacts as the epoxy did not stick well to the wire, and so had to place them by hand. Though this made the contacts larger than desirable, the tradeoff for mechanical robustness was worth it. After placing the epoxy and wire on the graphene, we heated-up the sample in the thermal annealer, set to 150° C, for twenty minutes. After the epoxy had been set, we experienced none of the problems encountered earlier with the weak silver-paint contacts.

To create backgate contacts, we chose to create contact from the top of the chip. We scratched off a little bit of the oxide on the edge of the chip using a diamond scribe, and then placed indium solder on top. We then attached a gold wire to the solder. We sometimes encountered difficulties forcing the indium to stick to the top of the chip, especially when the sample was a little dirty. One effective trick seemed to be to let the indium spill over the edge of the chip.

When the sample was fully prepared, we placed it on a dip socket, placing a small amount of vacuum grease in between in order to keep the sample in place. The wires were then soldered (with indium solder) to the pins of the socket, oftentimes using flux on the wires and pins to keep the solder on.

In some of the measurements we chose to anneal our sample in order to improve its electrical quality. We used the lab's thermal annealer in order to accomplish this. Reports from the Kong Group indicated that annealing could drastically shift the Dirac point of the sample, but that if the sample were exposed to air after annealing for even a minute's amount of time, the effect of the annealing would be reversed. Therefore, we had to take care that after annealing we kept the sample in an inert environment.

The process of annealing was accomplished as follows: First, after the sample had all of its contacts in place and was soldered onto a dip socket, we sealed the dip socket in the thermal annealer. We then flowed forming gas into the chamber for a few minutes to ensure that no air remained. The annealer was then set to a high temperature, usually between  $170^{\circ} - 200^{\circ}\text{C}$ , and left for six to ten hours. (It should be noted that the temperature setting of the annealer was not the temperature felt by the graphene; as the graphene was sitting on a dip-socket, it was in poor thermal contact with the heating strip. We found that indium on the top of the chip started to melt when the thermal annealer was set to  $205^{\circ}\text{C}$ , which allowed us to conclude that the 'effective' temperature the chip was experiencing at this setting was actually only  $150^{\circ}\text{C}$  (the melting point of indium). We thus set our annealer to heat the sample at an effective temperature of  $100 - 150^{\circ}\text{C}$ .)

When we were ready to take the sample out, we placed a large clear bag over the top of the annealer and flowed nitrogen through it. We then took the sample out of the annealer and placed it on the end of a dewar stick. The dewar stick had previously been vacuumed and then flowed with nitrogen. Once the sample was sealed into the stick, we pumped the stick to vacuum before transferring to the dilution fridge.

## 2.5 Experimental Setup

Our experimental setup is shown in Figure 2-3. We placed the dip-socket to which we had connected our sample on a long stick which we then lowered into the lab's dilution fridge. With the sample in the dilution fridge, we could perform measurements at

room temperature, 77 Kelvin (nitrogen temperature), 4 K (Helium temperature) and 100 mK (with the 1-K pot running).

To carry out the four probe measurements discussed above, we used a 7280 DSP Lock-in Amplifier and a lab-made DC voltage box. A 1 Volt signal at 13.156 Hz was output from the lock-in and put through a  $1 \text{ M}\Omega$  resistor, creating an effective current of magnitude  $1 \mu\text{A}$ . We then connected this current to one of the four graphene leads, and ground one of the other leads to create our  $I_{in}$  and  $I_{out}$ . We then attached leads to the other two contacts and used them as input to the lock-in (these were our  $V_A$  and  $V_B$  contacts). We had to adjust the phase between the reference signal (the output of the lock-in) and the input signal in order to ‘zero’ out the lock-in, i.e. get the signal entirely in the ‘x’ component of the lock-in. We then recorded the measurements of the lock-in, which told us the voltage difference between  $V_A$  and  $V_B$ . (It should be noted that we were encountering some difficulties with the lock-in adding some constant offset to the signal making it impossible to put all the signal into the x component. This ended up being due to the AC gain on the lock-in being set too low and was fixed by adjusting this parameter on the lock-in).

In order to create a bias on the backgate, we connected one of the backgate contacts to our lab’s DC voltage box. The DC voltage box only outputs voltages between -10 and 10 V, so when higher voltages were desired, we hooked up the output of the DC voltage box to a Kepco bipolar operational power supply (model BOP 500M), the output of which was then hooked up to the backgate contact. To prevent too large of a voltage from being applied, we put a voltage divider at the output of the power supply to limit the maximum amount of voltage that went through. We also added a  $10 \text{ M}\Omega$  resistor to reduce the current.

## 2.6 Controlling the Experiment

We were able to control much of the experiment, as well as perform measurements, using the lab’s already in place system for communication with devices. The lock-in parameters, the voltage box outputs, and the magnetic field could all be changed

by a computer via GPIB or PIO cards. These communication tools were essential to performing automated measurements. We wrote scripts that swept the backgate voltage and the magnetic field as desired and wrote the lock-in measurements at each point to a file.

## 2.7 Experimental Parameters

We took two different types of data sweeps for this study. In the first, we set a fixed magnetic field and swept the backgate voltage. The fixed fields at which we took data were +10 T, -10 T, +4 T, -4 T, and 0 T (all but the latter 4 K, with the 0 T data at 77 K). The second type of measurement involved setting the backgate voltage to a fixed value, and sweeping the magnetic field. In this case, we took data at fixed backgate voltages of 0 V (100 mK), 25 V, and 55.6 V (both at 4 K). (Unfortunately, we were not able to complete the full set of measurements at each temperature due to a backgate leakage that occurred during measurements and an inability to make a new sample within the time-span of this project.)

In total, we studied four different configurations (see Figure 2-4 and 2-5). Two configurations were the parallel configurations needed for the VDP measurement, while the other two were the cross configurations. In order to specify which configuration the sample was in, we will place subscripts on the quantity being measured (the quantity being either voltage  $V$  or resistance  $R=V/1\mu A$ ); the first two indices will mark the contacts being used for  $I_{in}$  and  $I_{out}$ , while the second two indices will indicate the contacts used for  $V_A$  and  $V_B$ . Thus  $V_{14,23}$  gives the voltage measured when contact 1 was  $I_{in}$ , 4 was  $I_{out}$ , 2 was  $V_A$  and 3 was  $V_B$ .

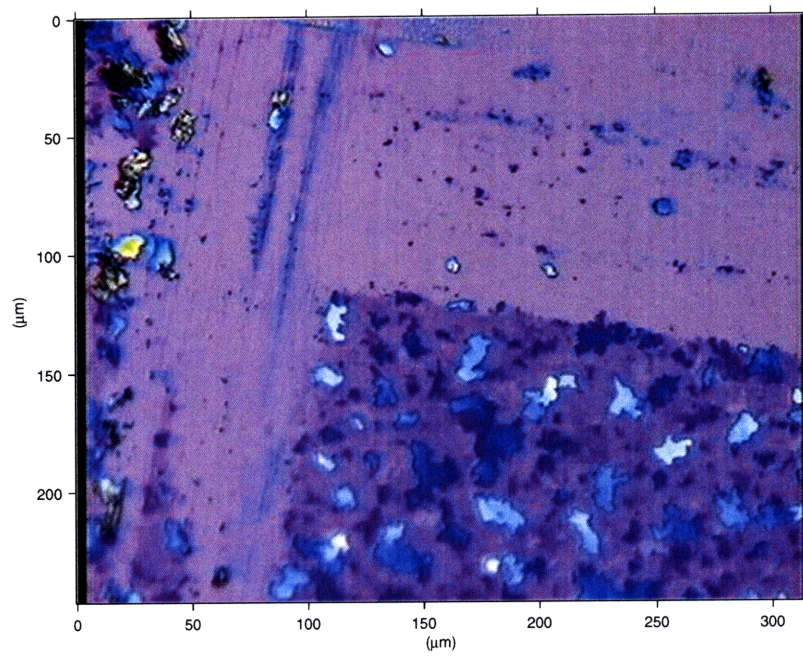


Figure 2-2: Optical image of a piece of graphene scraped to suit our measurement needs.

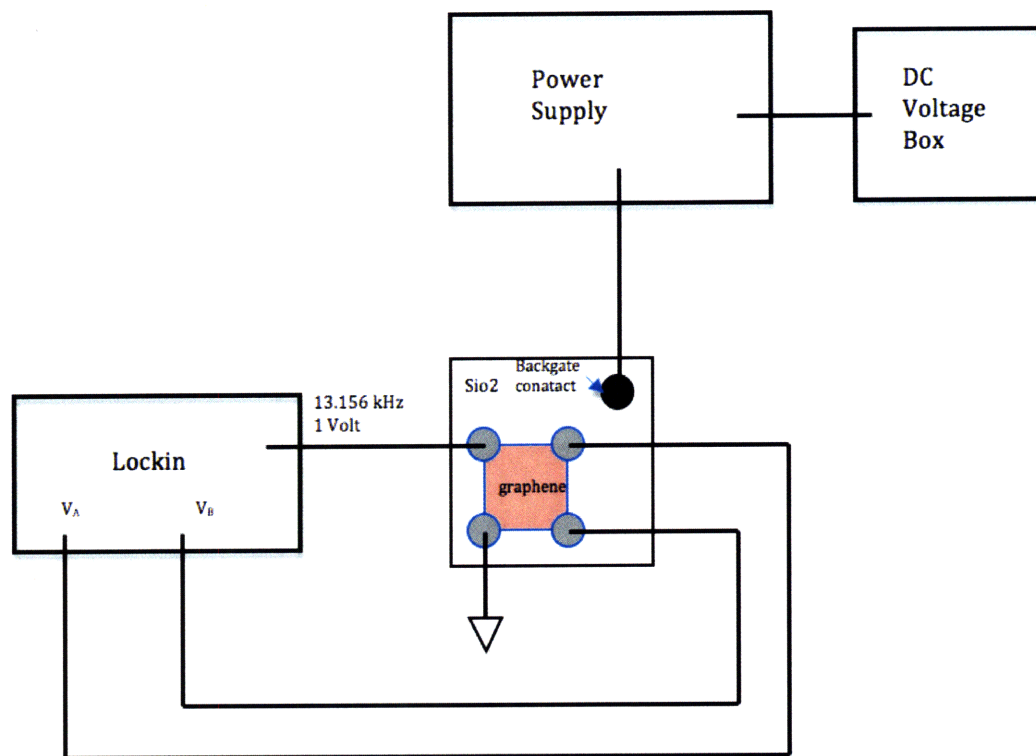


Figure 2-3: Here we show a representation of our experimental setup. The lock-in signal output was sent to one of the graphene contacts, with another contact grounded. The remaining two contacts provided our voltage signal, measured by the lock-in. The backgate was biased to change the makeup of the charge carriers.

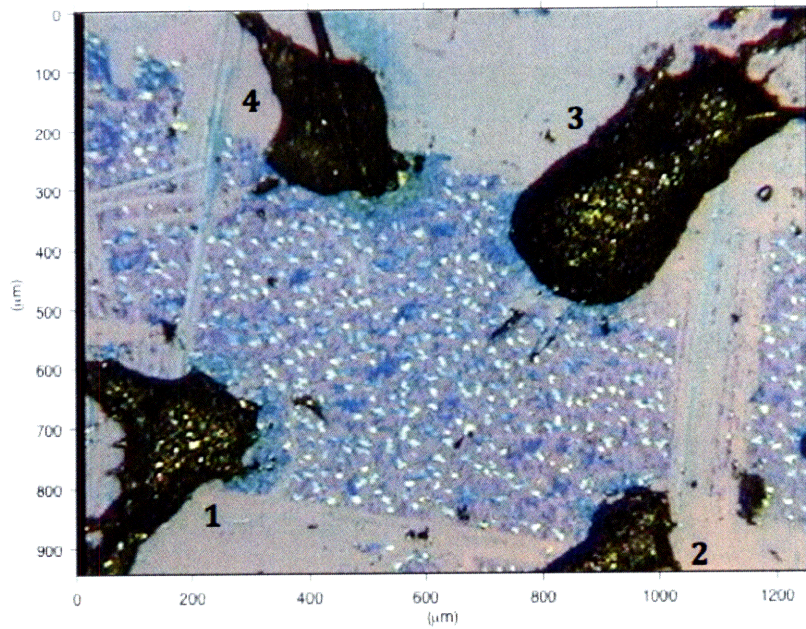


Figure 2-4: The graphene sample used for these studies, with the four silver-epoxy contacts labeled. Scale is in microns.

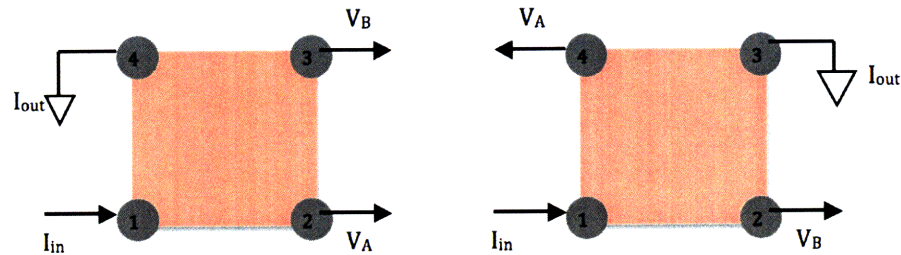


Figure 2-5: Two measurement configurations shown for a VDP measurement  $V_{14,23}$  on the left and a cross measurement  $V_{13,42}$  on the right. The other two, not shown, were the second VDP configuration ( $V_{12,43}$ ) and the second crossed configuration ( $V_{24,31}$ ).

# Chapter 3

## Results

### 3.1 Raw Data

#### 3.1.1 Voltage Sweeps

Below we include some of the raw data for the VDP measurements (Figures 3-1 and 3-2).

We make the following notes about the data:

1. The longitudinal resistivity does not drop to zero at any point, as would be expected for a sample exhibiting quantum Hall effect.
2. One can extract the Dirac point from each of the VDP measurements by taking it to be the voltage at which the maximal longitudinal signal is measured. However, it becomes clear that this Dirac point is at different locations for different measurement configurations, and so it becomes hard to declare one voltage as being the charge neutrality point. For example, for the  $V_{14,23}$  measurements, the peak occurs at -5.6 V at 0 T (77°), at -8.3 V at 4 T, -13.6 V at 10 T, 5.3 V at -4 T, and 8.3 at -10 T. The Dirac peak similarly shifts around for  $V_{14,23}$  measurements.
3. Shoulders or ‘bumps’ appear in the curves at all fields (even zero field). For example, in the  $V_{14,23}$  measurement, we see some sort of structure appear  $\sim 20$

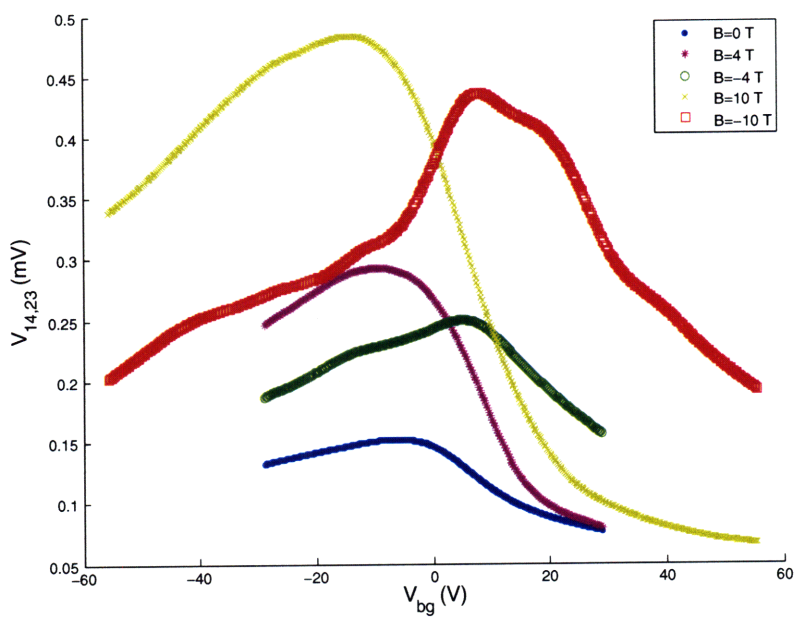


Figure 3-1: Raw data for the first VDP configuration,  $V_{14,23}$ .

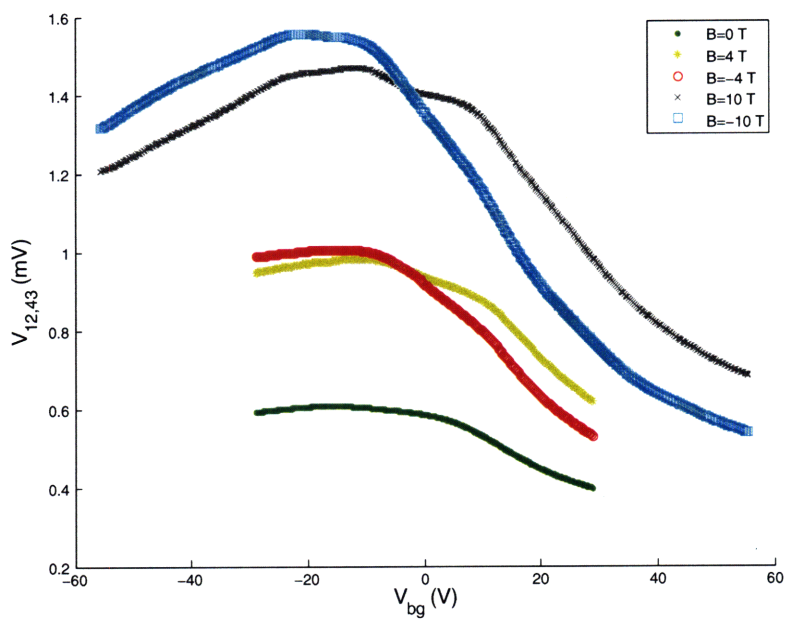


Figure 3-2: Raw data for the second VDP configuration,  $V_{14,23}$ .

$V$  below the Dirac point at both -4 and -10 T, while the  $V_{14,23}$  measurement has shoulders 19-20 V above the Dirac point at 4 and 10 T. However, other shoulders appear in the data that are not in multiples of 20 V away from the Dirac point.

4. Some of the traces seem to exhibit two Dirac points, i.e. two closely maxima of almost equal height. This is especially true for the highest field measurements.

We include below the crossed measurements in Figures 3-3 and 3-4. We point out the most salient features of these crossed traces:

1. Since we are measuring  $V_H$ , we expect that the measurement changes sign at the Dirac point, where the sign of the charge carriers changes. No such change in sign is seen.
2. Though one expects  $V_H$  to become large when the number of charge carriers goes to zero, no such ‘blowing up’ of the measured voltage appears in the traces.
3. No quantum Hall plateaus can be seen in the measurements.
4.  $V_{13,42}$  at +10 T (+4 T) lines up exactly with  $V_{24,31}$  at -10 T (-4 T). Similarly,  $V_{24,31}$  at +10 T (+4 T) lines up (to within the noise) with  $V_{13,42}$  at -10 T (-4 T). This property is known in the literature as an outcome of the Reciprocity Theorem which states that

$$V_{nm,jk}(B) = V_{jk,nm}(-B). \quad (3.1)$$

The Reciprocity Theorem is still valid even for inhomogeneous samples where irregular current patterns mix the  $\rho_{xx}$  and  $\rho_{xy}$  measurements. (See [21], [24], and [4]).

5. At positive magnetic fields,  $V_{13,42}$  looks similar to the VDP measurements, exhibiting a maximum. At negative magnetic fields, we see more reasonable behavior for a cross configuration with an asymmetric trace with no maximum.

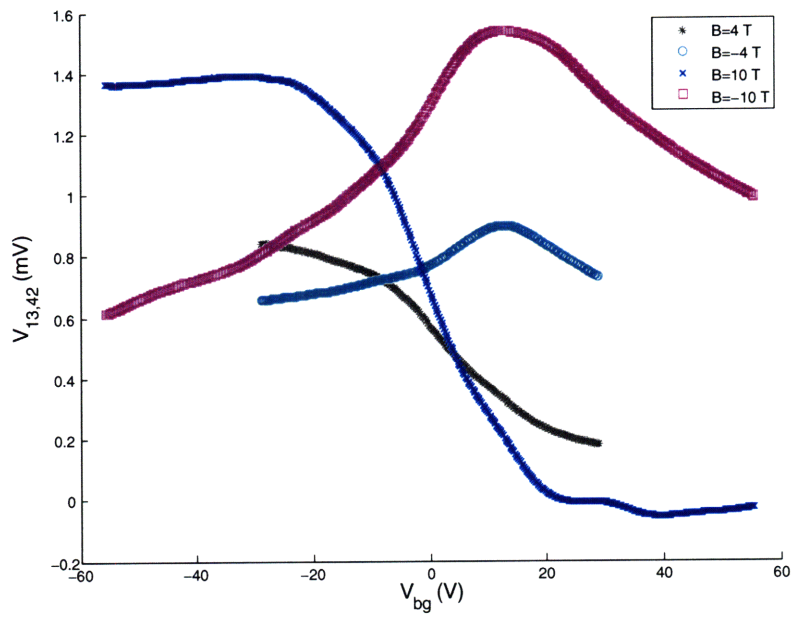


Figure 3-3: Raw data for the first crossed configuration,  $V_{13,42}$ .

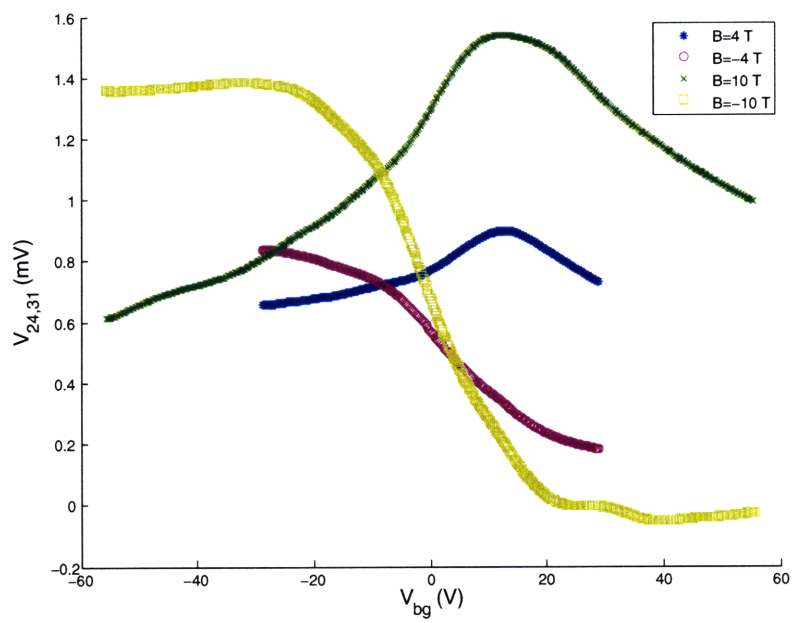


Figure 3-4: Raw data for the second crossed configuration,  $V_{24,31}$ .

The opposite is true for  $V_{24,31}$ (meaning, the asymmetric behavior is exhibited at positive fields).

### 3.1.2 Magnetic Field Sweeps

We performed magnetic field sweeps, setting the backgate voltage to a specific value and then changing the field from -10 T to 10 T. We note that there are no clear Shubnikov- de Haas oscillations in any of the configurations (see Figure 3-5). We also note that all traces have marked increases in resistance zero field. This cusp was seen at all backgate voltages swept and increased in magnitude as the temperature was lowered. This increase in the magneto-resistance is indicative of the sample exhibiting weak localization, and not weak anti-localization.

## 3.2 Symmetrization and Antisymmetrization Averaging

As pointed out above, the crossed configurations do not show the correct behavior. In addition, the longitudinal configurations do not give the same bias value for the Dirac point. This created serious difficulty for further characterization of the material. It seemed that due to the inhomogeneity of the sample and the misalignment of the contacts, the two measurements of  $\rho_{xx}$  and  $\rho_{xy}$  became mixed.

In an attempt to separate these two quantities, we performed symmetrization and antisymmetrization averaging over the magnetic field. What we mean by this is as follows: one expects that  $\rho_{xx}$  is independent of the sign of the magnetic field, while  $\rho_{xy}$  is antisymmetric with respect to the field. Thus if we take the symmetric average of a VDP configuration at a field  $B$  and its negative  $-B$ , meaning  $\rho_{xx}^{sym} = \frac{1}{2}[\rho_{xx}(B) + \rho_{xx}(-B)]$ , we expect that any contribution that is due to  $\rho_{xy}$  will cancel out, leaving only the true  $\rho_{xx}$ . Similarly, if we take the antisymmetric average of  $\rho_{xy}$ , i.e.  $\rho_{xy}^{antisym} = \frac{1}{2}[\rho_{xy}(B) + \rho_{xy}(-B)]$ , we expect the longitudinal part of the measurement that we accidentally recorded to be cancelled out.

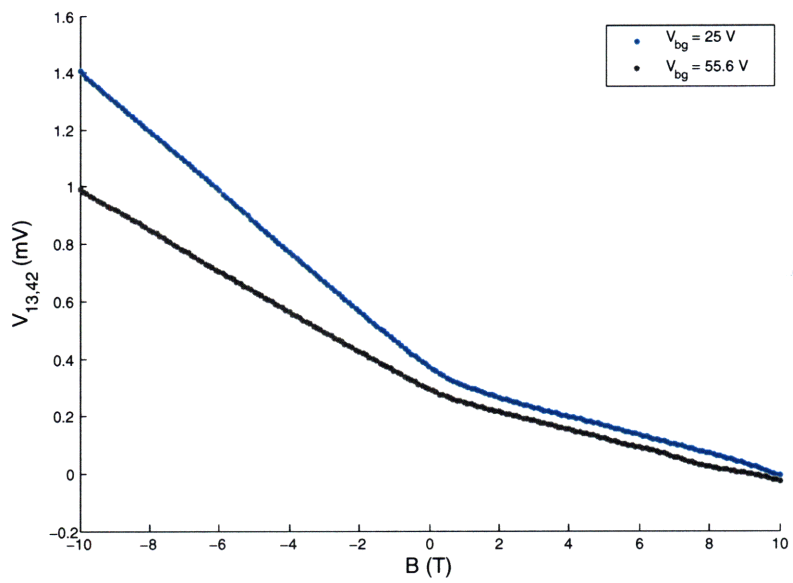


Figure 3-5: Raw data for magnetic sweep at two backgate voltages,  $V_{bg}=55.6 \text{ V}$  and  $V_{bg}=25 \text{ V}$ , both measuring  $V_{24,31}$ .

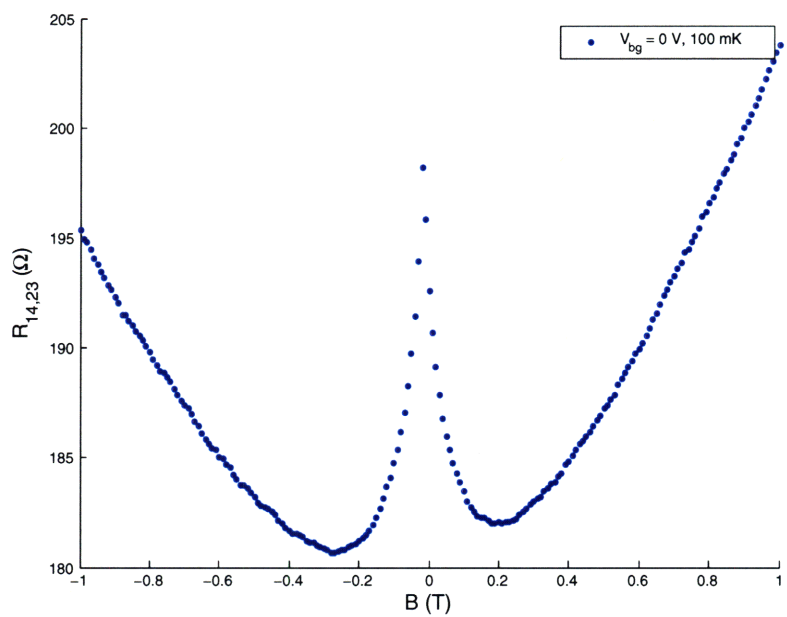


Figure 3-6: Weak localization effect seen at zero backgate voltage at 100 mK.

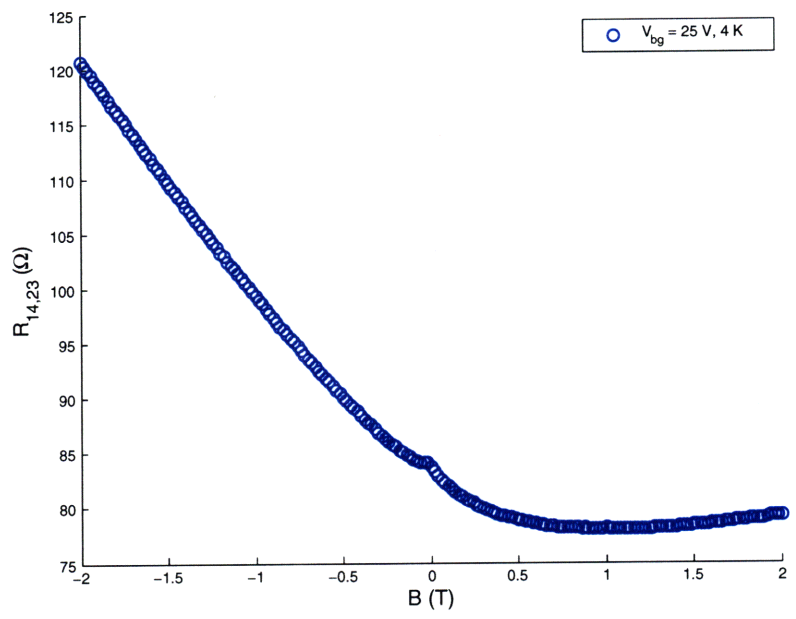


Figure 3-7: Weak localization effect seen at  $V_{bg}=25$  V at 4 K.

This method is a somewhat naive approach to fixing the mixing problem, as one cannot know that the  $\rho_{xx}$  measured is completely symmetric in magnetic field [24]. Nevertheless, it provides us with a method of determining the Dirac point. As pointed out above, no clear Dirac point can be found from the VDP measurements. However, if we look at the antisymmetrization of the cross configurations, one finds that they all go through zero at a backgate voltage of -8.3 V (see Figure 3-8), suggesting that the Dirac point is located at this bias voltage.

### 3.3 Annealing Effects

We performed resistance measurements as a function of voltage on the graphene both before and after annealing at zero magnetic field. In both cases we were able to identify the Dirac peak of the sample. The sample prior to annealing was found to have a Dirac point on the electron-side of the spectrum, at a value between 65-80 V. After annealing, the Dirac point was markedly shifted to the hole-side, residing at a value of -8.3 V. This confirms what other groups have found with annealing improving the sample quality.

### 3.4 Mobility Measurements

To determine the mobility, we first tried to use the VDP and Hall measurements as described in Chapter 2. By obtaining  $R_S$ , the sheet resistance, via the VDP measurement, and  $n$ , the sheet carrier density, from the Hall measurements, we would then have the mobility:  $\mu = \frac{1}{qR_S n}$ . However, using this method proved to be difficult due to the Hall configuration traces. As mentioned above, the Hall configuration traces do not have the expected form: they do not go to  $\pm\infty$  at the Dirac point, so using these traces to obtain  $n$  did not give sensible results.

Therefore, we decided to calculate the mobility solely from the VDP measurements. We obtained  $R_S$  as was prescribed by the VDP measurements (Figure 3-9). To obtain  $n$ , we used a simple capacitance model of the Si/SiO<sub>2</sub>/graphene system to

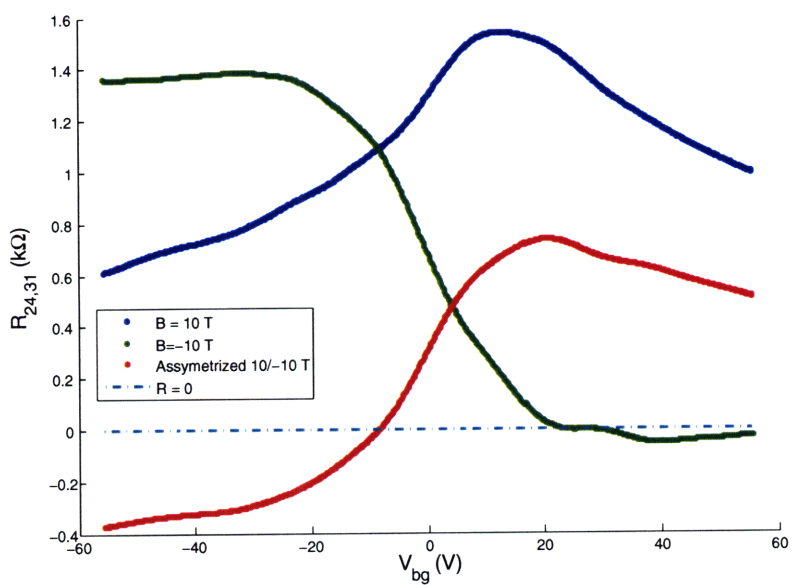


Figure 3-8:  $V_{24,31}$  data for +10 T, -10 T, and the antisymmetrized average of the two.

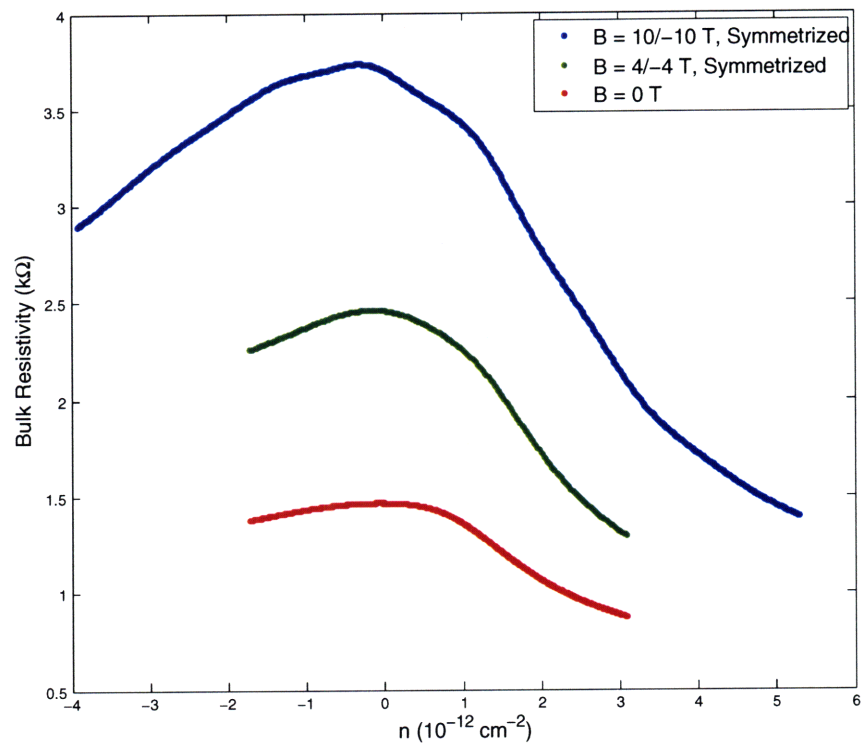


Figure 3-9: Sheet resistance  $R_S$  evaluated with the symmetrized VDP averages.

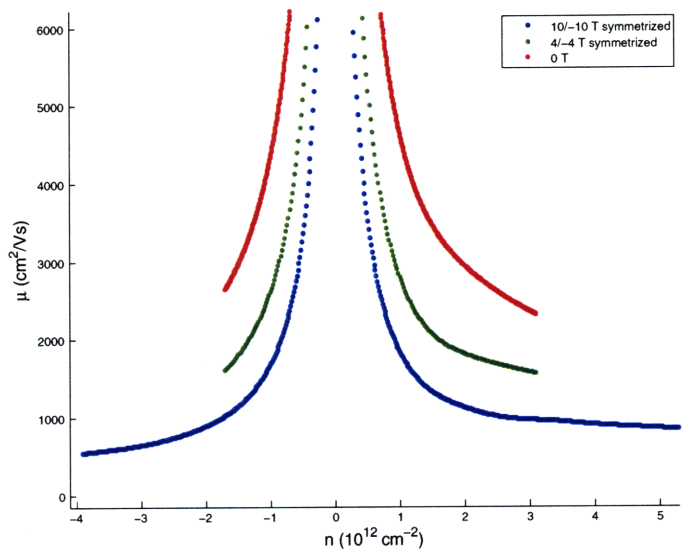


Figure 3-10: Mobility calculated via the VDP traces as a function of the density. While mobility really only carries meaning at zero field, we here also show the mobility derived at 10 and 4 T to show the large density behavior.

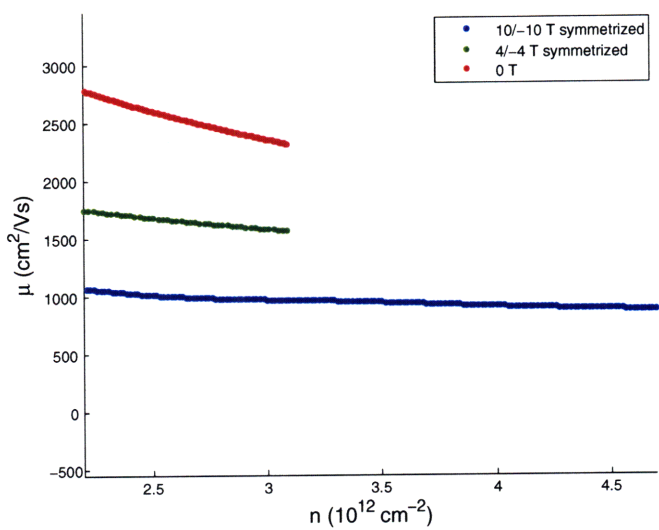


Figure 3-11: Mobility calculated via the VDP traces on the electron side.

calculate how much charge was being induced on the sample. Thus we have

$$Q_S = C_S V_{bg} \quad (3.2)$$

where  $Q_S = qn$  is the total sheet charge induced (in units of Coulombs/cm<sup>2</sup>),  $C_S$  is the capacitance per area of the silicon dioxide layer (F/cm<sup>2</sup>), and  $V_{bg}$  is the backgate voltage applied. For SiO<sub>2</sub> of thickness 300 nm one finds  $C_S = 1.15 \times 10^{-10} F/cm^2$ . This yields an increase in the number density  $n$  by  $7.18 \times 10^{10}$  per volt applied to the backgate. We assumed that the Dirac point was at -8.3 V, the result from our antisymmetrization of the cross configurations. We then plotted  $R_S$  as a function of  $n$ , where  $n$  was set to zero at  $V_{bg}= 8.3$  V. The mobility as a function of the density is plotted in Figure 3-10, with a close up of the electron side in Figure 3-11. In general, the mobility of a sample is a quantity that is measured at zero magnetic field, but we also show the ‘mobility’ (i.e.  $\mu(B) = \frac{1}{qR_S(B)n}$ ) at two non-zero magnetic field strengths. Our motivation in including these is that we lack sufficient data to see the high-density behavior of the mobility at zero field, so by looking at the ‘milities’ for non-zero magnetic fields we can get a qualitative sense of the behavior at zero field. In studies carried out by the Kong Group on the large-area graphene samples, the mobility of samples was found to range between 100-2000 cm<sup>2</sup>/Vs, in good agreement with our results and at least an order of magnitude smaller than the mobilities achieved by most monolayer graphene samples [25]. However, we do not have an explanation for the difference between the hole and electron mobilities that can be seen in our data, especially at higher fields. One conjecture to explain this phenomenon is that the effect of annealing on electron conduction is much more dramatic than on hole conduction, but we did not have enough data at room temperature before annealing to confirm this hypothesis.

### 3.5 Shubnikov-de Haas Oscillations

One of the main goals of this study was to learn if the large-scale sample exhibited quantum Hall characteristics as seen in monolayer graphene. Looking at the data from the voltage sweeps, the answer to this question is not immediately obvious. We do not see the characteristic plateaus of the crossed configurations or the zeros in the longitudinal resistance. Although there are bumps in the data, these bumps appear at all fields (even zero field), so it is hard to associate them with the quantum Hall effect. In addition, they appear at much lower values than would be expected for the first few plateaus. For example, the asymmetrized crossed configurations of the 10 and -10 T fields (see Figure 3-8) show some kind of feature at  $0.65 \text{ } k\Omega$ , or in terms of the conductance,  $1.5 \times 10^{-3}$  Siemens. Since the conductance plateaus in graphene occur at  $(n + 1/2)\frac{4e^2}{h}$ , if this feature were actually a plateau it would be the 9th or 10th plateau. It seems improbable that the disorder washed out the first 8 plateaus, so we cannot conclude that we are seeing a true quantum Hall plateau.

If the sample were exhibiting quantum Hall characteristics, we would expect the Hall voltage to be periodic in  $1/B$ , where  $B$  is the magnetic field applied. The period of oscillations (in units of inverse of the magnetic field) can be related to the density of the carriers  $n$  as follows:

$$n = \frac{4}{\Phi_0 \Delta(1/B)} \quad (3.3)$$

where  $\Phi_0$  is the unit of flux and  $\Delta(1/B)$  is the period in inverse magnetic field.

To check this, we took our magnetic field sweep data and plotted it as a function of the inverse of the magnetic field. No oscillations were seen in this data, but looking at the derivative of our data (or the difference between every pair of subsequent points), clear oscillations emerged in the inverse field. We carried out a Fourier transform of the derivative of our measurements to determine the period. For the  $V_{13,42}$  sweep with  $V_{bg} = 55.6 \text{ V}$  (and examining the asymmetrized version), we found a period of  $0.05 \text{ } T^{-1}$ . This corresponds to a density of  $n = 1.9 \times 10^{12} \text{ cm}^{-2}$ . The expected value, however, calculated via the capacitance model with -8.3 V as the Dirac point,

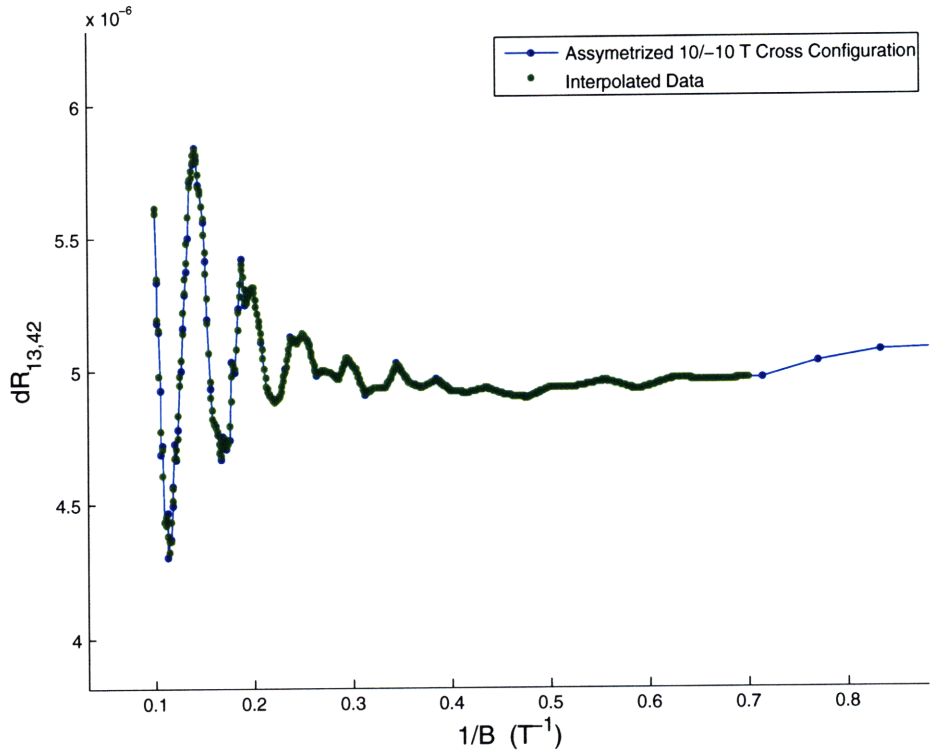


Figure 3-12: The difference between subsequent data points in  $R_{xy}$  (for  $V_{bg} = 50$  V) plotted as a function of the inverse magnetic field. The green is interpolated data, needed in order to have evenly spaced data in inverse magnetic field for the fourier transform.

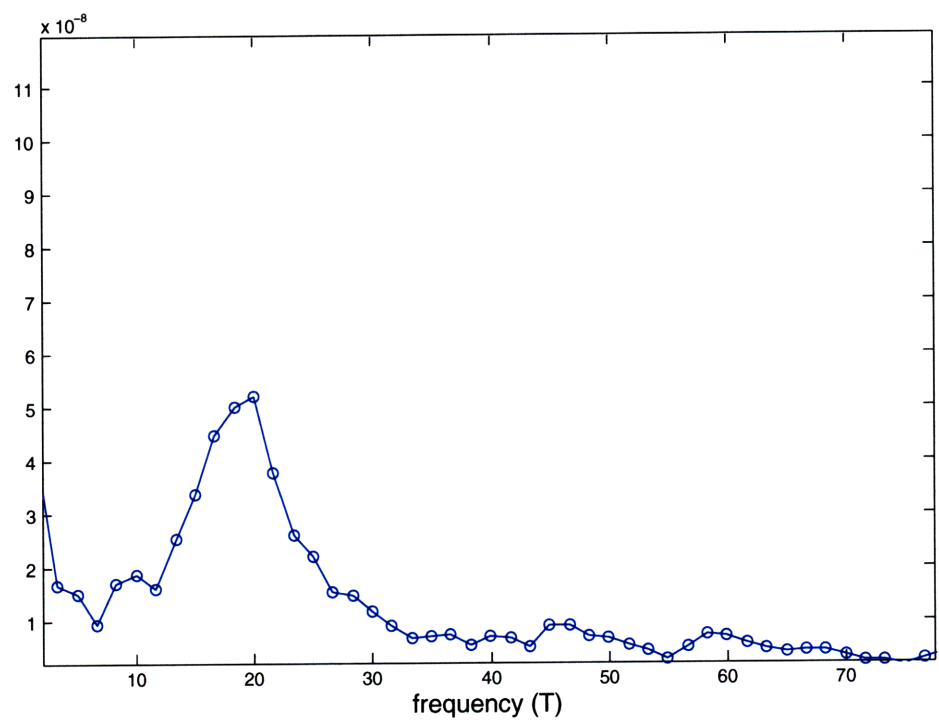


Figure 3-13: Fourier transform of the data shown in Figure 3-12

was  $n = 4.5 \times 10^{12} cm^{-2}$ . Similarly, for the sweep taken at  $V_{bg} = 25$  V, we find  $\Delta(1/B) = 0.1 T^{-1}$ , yielding  $n = 9.8 \times 10^{11} cm^{12}$ . The expected value from the capacitance model is again higher, being  $n = 2.3 \times 10^{12} cm^{-2}$ . The sweep that we took with  $V_{bg} = 0$  V was not periodic in the inverse magnetic field, indicating that one needs higher densities to be able to see the oscillations.

The fact that the oscillations yield such low values for the densities forces us to conclude that although there are characteristic oscillations, the role of the disorder in the sample cannot be neglected. The effect of having regions with multiple layers of graphene clearly has an effect on the quantum characteristics of the material.

# Chapter 4

## Conclusion

### 4.1 Future Studies

Due to the limited time scope of this project, we were not able to explore the system as fully as would be desired. A more thorough study of CVD-grown graphene is needed to provide a more complete picture of the properties measured in this thesis (mobility, oscillations, weak localization effects). More magnetic field sweeps at different backgate values should be performed so as to get a better understanding of the Shubnikov-de Haas oscillations. In addition, all measurements should be carried out at all available temperatures so that the temperature dependence of properties can be better understood. Another direction of study should focus on understanding how changing the size of the sample changes the outcome of these measurements.

### 4.2 Summary

In conclusion, we have performed a set of transport measurements on CVD-grown graphene. Despite difficulties with mixing between the longitudinal and crossed signals, we are able to characterize the mobility of the sample and to conclude that mobility of these samples is much smaller than the mobility of single-layer graphene. In addition, though we see oscillations in the magnetoresistance traces, we find that these oscillations do not give exactly the correct number density, forcing us to believe

that the disorder in the sample plays a significant role.

# Bibliography

- [1] Cristina Bena and Gilles Montambaux. Remarks on the tight-binding model of graphene, 2007.
- [2] Claire Berger, Zhimin Song, Xuebin Li, Xiaosong Wu, Nate Brown, Cecile Naud, Didier Mayou, Tianbo Li, Joanna Hass, Alexei N. Marchenkov, Edward H. Conrad, Phillip N. First, and Walt A. de Heer. Electronic Confinement and Coherence in Patterned Epitaxial Graphene. *Science*, 312(5777):1191–1196, 2006.
- [3] K.I. Bolotin, K.J. Sikes, Z. Jiang, M. Klima, G. Fudenberg, J. Hone, P. Kim, and H.L. Stormer. Ultrahigh electron mobility in suspended graphene. *Solid State Communications*, 146(9-10):351 – 355, 2008.
- [4] M. Büttiker. Symmetry of electrical conduction. *IBM J. Res. Dev.*, 32(3):317–334, 1988.
- [5] K. S. Kim et. al. Large-scale pattern growth of graphene films for stretchable transparent electrodes. *Nature*, 457:706–710.
- [6] K. S. Novoselov et. al. Two-dimensional gas of massless dirac fermions in graphene. *Nature*, 438(5817):197–200, 2005.
- [7] Novoselov K.S. Geim, A. K. The rise of graphene. *Nature*, 2007.
- [8] E. H. Hall. On a new action of the magnet on electric currents. *American Journal of Mathematics*, 2:287–292, 1879.
- [9] M. I. et. al. Katsnelson. Chiral tunneling and the klein paradox in graphene. *Nature Physics*, 2006.
- [10] Mikhail I. Katsnelson. Graphene: carbon in two dimensions. *Materials Today*, 10(1-2):20 – 27, 2007.
- [11] O. Klein. Die reexion von elektronen an einem potentialsprung nach der relativistischen dynamik von dirac. *Z. Phys.*, 1929.
- [12] L. D. Landau and E. M. Lifshitz. *Statistical Physics, Part I*. Pergamon, Oxford, 1980.
- [13] NIST Website: <http://www.eeel.nist.gov/812/effe.htm#vand>.

- [14] S. V. Morozov, K. S. Novoselov, M. I. Katsnelson, F. Schedin, D. C. Elias, J. A. Jaszczałk, and A. K. Geim. Giant intrinsic carrier mobilities in graphene and its bilayer. *Physical Review Letters*, 100(1):016602, 2008.
- [15] A. H. Castro Neto, F. Guinea, N. M. R. Peres, K. S. Novoselov, and A. K. Geim. The electronic properties of graphene. *Reviews of Modern Physics*, 81(1):109, 2009.
- [16] K. S. Novoselov, A. K. Geim, S. V. Morozov, D. Jiang, Y. Zhang, S. V. Dubonos, I. V. Grigorieva, and A. A. Firsov. Electric Field Effect in Atomically Thin Carbon Films. *Science*, 306(5696):666–669, 2004.
- [17] K. S. Novoselov, D. Jiang, F. Schedin, T. J. Booth, V. V. Khotkevich, S. V. Morozov, and A. K. Geim. Two-dimensional atomic crystals. *Proceedings of the National Academy of Sciences of the United States of America*, 102(30):10451–10453, 2005.
- [18] K. S. Novoselov, Z. Jiang, Y. Zhang, S. V. Morozov, H. L. Stormer, U. Zeitler, J. C. Maan, G. S. Boebinger, P. Kim, and A. K. Geim. Room-Temperature Quantum Hall Effect in Graphene. *Science*, 315(5817):1379–, 2007.
- [19] A.N. Obraztso. Chemical vapor deposition: making graphene on a large scale. *Nature Nanotechnology*, 4:212.
- [20] Taisuke Ohta, Aaron Bostwick, Thomas Seyller, Karsten Horn, and Eli Rotenberg. Controlling the Electronic Structure of Bilayer Graphene. *Science*, 313(5789):951–954, 2006.
- [21] H. M. Pastawski and E. Medina. Tight binding methods in quantum transport through molecules and small devices: From a coherent to a decoherent description. *Revista Mexicana de Física*, 46:1, 2001.
- [22] Van der Pauw. A method of measuring specific resistivity and hall effect of discs of arbitrary shape. *Philips Research Report*, 13:1–9, 1958.
- [23] P. S Peercy. The drive to miniaturization. *Nature*, 406:1023–1026, 2000.
- [24] E. Peled, D. Shahar, Y. Chen, D. L. Sivco, and A. Y. Cho. Observation of a quantized hall resistivity in the presence of mesoscopic fluctuations. *Phys. Rev. Lett.*, 90(24):246802, Jun 2003.
- [25] Alfonso Reina, Xiaoting Jia, John Ho, Daniel Nezich, Hyungbin Son, Vladimir Bulovic, Mildred S. Dresselhaus, and Jing Kong. Large area, few-layer graphene films on arbitrary substrates by chemical vapor deposition. *Nano Letters*, 9(1):30–35, 2009.
- [26] C. Schonenberger. Bandstructure of graphene and carbon nanotubes: An exercise in condensed matter physics, 2000. This is a full MISC entry.
- [27] P. R. Wallace. The band theory of graphite. *Phys. Rev. Lett*, 71:633–634, 1947.